

Electronic ISSN: 1309-0267



**International Journal
of Engineering &
Applied Sciences**

**I
J
E
A
S**

IJEAS

**Volume 16, Issue 1
2024**

Published by Akdeniz University

HONORARY EDITORS

(in alphabetical order)

- Prof. Atluri, S.N.- University of California, Irvine-USA
Prof. Liew, K.M.- City University of Hong Kong-HONG KONG
Prof. Lim, C.W.- City University of Hong Kong-HONG KONG
Prof. Liu, G.R.- National University of Singapore- SINGAPORE
Prof. Nath, Y.- Indian Institute of Technology, INDIA
Prof. Omurtag, M.H. -ITU
Prof. Reddy, J.N.-Texas A& M University, USA
Prof. Saka, M.P.- University of Bahrain-BAHRAIN
Prof. Shen, H.S.- Shanghai Jiao Tong University, CHINA
Prof. Xiang, Y.- University of Western Sydney-AUSTRALIA
Prof. Wang, C.M.- National University of Singapore- SINGAPORE
Prof. Wei, G.W.- Michigan State University-USA

EDITOR IN CHIEF:

Assoc. Prof. Ibrahim AYDOGDU -Akdeniz University aydogdu@akdeniz.edu.tr

ASSOCIATE EDITORS:

Assist. Prof. Kadir MERCAN –Mehmet Akif Ersoy
University kmercan@mehmetakif.edu.tr

SECTION EDITORS:

- Assoc. Prof. Metin Mutlu Aydın – Ondokuz Mayıs University
Assoc. Prof. Mustafa Arda –Trakya University
Assist. Prof. Refik Burak Taymuş- Van 100. Yıl University

EDITORIAL BOARD

(The name listed below is not Alphabetical or any title scale)

Prof. Xinwei Wang -Nanjing University of Aeronautics and Astronautics

Asst. Prof. Francesco Tornabene -University of Bologna

Asst. Prof. Nicholas Fantuzzi -University of Bologna

Assoc. Prof. Keivan Kiani - K.N. Toosi University of Technology

Asst. Prof. Michele Baccocchi -University of Bologna

Asst. Prof. Hamid M. Sedighi -Shahid Chamran University of Ahvaz

Prof. Yaghoub Tadi Beni -Shahrekord University

Prof. Raffaele Barretta -University of Naples Federico II

Prof. Meltem ASİLTÜRK -Akdeniz University *meltemasilturk@akdeniz.edu.tr*

Prof. Metin AYDOĞDU -Trakya University *metina@trakya.edu.tr*

Prof. Ayşe DALOĞLU - KTU *aysed@ktu.edu.tr*

Prof. Oğuzhan HASANÇEBİ - METU *oguzhan@metu.edu.tr*

Asst. Prof. Rana MUKHERJİ - The ICFAI University

Assoc. Prof. Baki ÖZTÜRK - Hacettepe University

Assoc. Prof. Yılmaz AKSU -Akdeniz University

Assoc. Prof. Hakan ERSOY- Akdeniz University

Assoc. Prof. Mustafa Özgür YAYLI -Uludağ University

Assoc. Prof. Selim L. SANİN - Hacettepe University

Asst. Prof. Engin EMSEN -Akdeniz University

Prof. Serkan DAĞ - METU

Prof. Ekrem TÜFEKÇİ - İTÜ

ABSTRACTING & INDEXING



IJEAS provides unique DOI link to every paper published.

EDITORIAL SCOPE

The journal presents its readers with broad coverage across some branches of engineering and science of the latest development and application of new solution algorithms, artificial intelligent techniques innovative numerical methods and/or solution techniques directed at the utilization of computational methods in solid and nano-scaled mechanics.

International Journal of Engineering & Applied Sciences (IJEAS) is an Open Access Journal

International Journal of Engineering & Applied Sciences (IJEAS) publish original contributions on the following topics:

Civil Engineering: numerical modelling of structures, seismic evaluation, experimental testing, construction and management, geotechnical engineering, water resources management, groundwater modelling, coastal zone modelling, offshore structures, water processes, desalination, waste-water treatment, pavement and maintenance, transport and traffic, laser scanning, and hydrographic surveying, numerical methods in solid mechanics, nanomechanic and applications, microelectromechanical systems (MEMS), vibration problems in engineering, higher order elasticity (strain gradient, couple stress, surface elasticity, nonlocal elasticity)

Electrical Engineering: artificial and machine intelligence and robotics, automatic control, bioinformatics and biomedical engineering, communications, computer engineering and networks, systems security and data encryption, electric power engineering and drives, embedded systems, Internet of Things (IoT), microwaves and optics.

Engineering Mathematics and Physics: computational and stochastic methods, optimization, nonlinear dynamics, modelling and simulation, computer science, solid state physics and electronics, computational electromagnetics, biophysics, atomic and molecular physics, thermodynamics, geophysical fluid dynamics, wave mechanics, and solid mechanics.

Mechanical Engineering: machine design, materials science, mechanics of materials, manufacturing engineering and technology, dynamics, robotics, control, industrial engineering, ergonomics, energy, combustion, heat transfer, fluids mechanics, thermodynamics, turbo machinery, aerospace research, aerodynamics, and propulsion.

IJEAS allows readers to read, download, copy, distribute, print, search, or link to the full texts of articles.



CONTENTS

A Case Study of The Performance of A Pile-Supported Bracing Method for Basement Building

By Md. Alhaz Uddin, Mizanoor Rahman 1-15

Early Diagnoses of Acute Coroner Syndrome Based on Machine Learning Model

By Umut Utku Tiryaki, Gül Karaduman, Sare Nur Cuhadar, Ahmet Uyanik, Habibe Durmaz..... 16-32

Effect of Temperature on Damage Identification of Laminated Composite by Means Numerical Methods

By Bulent Ekici, Mehmet Ali Akın..... 33-43

Investigation of Pedestrian and Driver Behaviors at Push-Button Crosswalk on Main Arterials of Urban Roads : A Case of Samsun City, Türkiye

By Eren Dağlı, Ahmet Göktuğ Saraç, Metin Mutlu Aydın 44-62




A Case Study of The Performance of A Pile-Supported Bracing Method for Basement Building

Md. Alhaz Uddin^{a*}, Mizanoor Rahman^b

^aDepartment of Civil Engineering, College of Engineering, Jouf University, Sakaka-72388, Saudi Arabia

^bDepartment of Building Engineering and Construction Management, Khulna University of Engineering & Technology, Bangladesh.

✉: malhaz@ju.edu.sa^{a*}, mizan16@becm.kuet.ac.bd^b, : 0000-0002-1040-6034^{a*}, 0000-0001-6725-5989^b

Received: 15.08.2023, Revised: 14.01.2024, Accepted: 14.01.2024

Abstract

Deep excavations in urban areas are highly hazardous due to extensive settling of the surrounding soil, which can lead to the failure of retaining wall systems and the consequent collapse of adjoining properties. The retaining wall and bracing system are important for completing deep excavations for a basement building project. This paper evaluates the performance of an alternative, innovative, low-cost pile-supported bracing system (PSBS) method during excavation for two-level basement construction. Assessed PSBS performance in terms of ground settlement, lateral movement of supporting systems, schedule, and cost comparison. The PSBS excavation method was designed and then implemented to construct a two-level basement using the bottom-up method. The total station was utilized to monitor three-dimensionally, like the adjacent school building, ground surface settlement, and lateral movement of supporting systems. A schedule and cost comparison were performed using internal bracing and the PSBS technique. The recorded filed data was analysed, and it found that the lateral movement of the support system, adjacent building, and ground settlement is within the allowable limit. According to the estimated results, the PSBS method reduces construction time by 272 days compared to the internal bracing system. The PSBS approach is also less expensive than internal bracing for a two-level basement.

Keywords: Bracing system, excavation method, two-level basement, ground settlement, lateral movement.

1. Introduction

Deep excavation for basement construction of a building in the city area is always challenging because there are many types of risks, such as failure of the retaining wall system, excessive settlement of the surrounding structure or soil, and the collapse of adjacent properties. To prevent collapses during excavation for basement construction, various retaining walls, including sheet piles, contiguous bored piles, secant piles, internal or external bracing systems, and diaphragm walls, are required. Numerous investigations [1-4] are conducted to ensure the safety of the support system and surrounding structure during basement excavation using modelling, analytical techniques, and data collected on-site for a different technique. Among the most common excavation techniques are braced excavation, full open cut, island excavation, top-down construction, and anchored excavation.

The open excavation method is a method where no internal or external bracing system is required. It can be divided into slope open cut and cantilever open cut. This method is suitable for shallow excavation if sufficient space is available to maintain the required slope, but no bracing system is required. An internally supported excavation system uses horizontal bracing at the excavation side to resist the earth pressure from the back of the retaining wall. The bracing system includes a waler, strut, end bracing, and king post. The internal bracing system is the



most commonly utilized method for deep excavation [5]. A lot of research [6-9] was done on the internal bracing system, but it might be expensive for deep excavations, and this technology slows down the progress because it uses multiple bracing layers with permanent and temporary king posts. A deep tie-back excavation method was developed by Hudson et al. [10] and put into practice, although this approach necessitates additional raker footing, which is a difficult task.

An externally supported or anchored excavation system where the retaining wall is anchored externally. There are three segments of anchor excavation: the fixed section, the free section, and the anchor head. The function of the section is to provide anchoring force, transfer anchoring force to the anchoring head and lock the tendon, and transfer anchoring force to the structure, respectively. The anchoring method of excavation is also well-established, and numerous research had been conducted on it [7, 11]. This strategy, however, is appropriate when skilled workers and necessary machinery are unavailable.

Bottom-up basement construction method where excavation proceeds from ground level to the down until the formation level and casting proceeds from basement level to upward. The retaining wall, king post & bracing system are the basic components to execute the bottom-up method. In contrast, the top-down construction method is where the casting of permanent structures proceeds from ground level to down until the last basement completion. In this method, temporary openings keep facilitating excavation and casting works. The retaining wall & king post are the basic components required for this method [12]. The top-down method can reduce the construction time though the top-down method might cause more deflection of the retaining wall than the bottom-up method [13]. In the semi-top-down method slab at level 1 is used as a temporary working platform where the large opening is kept to carry out excavation. Level 1 slab acts as a frame to prevent lateral movement of the support system [14, 15]. Moreover, the combined top-down and bottom-up method central core zone is normally introduced bottom-up, and the perimeter portion proceeds with the top-down method, which has been implemented by Wang et al. [16].

There are lots of well-established excavation methods for basement construction. However, all the methods use a diaphragm wall, sheet pile, secant pile, or contiguous bored pile as a retaining wall. The internal or external bracing system with a king post was used to prevent movement of the retaining wall and surrounding facilities for a bottom-up method of basement construction. The high expenses and logistical difficulties associated with traditional bracing systems have prompted the investigation of alternative approaches to improve the cost-effectiveness and feasibility of construction projects.

However, this study is presented to evaluate the efficacy of an innovative, low-cost Pile Supported Bracing System (PSBS) in extremely soft and organic soil conditions. The original contribution of the proposed method is as follows: (i) evaluated the performance of PSBS by analysing ground settlement and lateral displacement of supporting systems; (ii) it introduced a low-cost pile-supported bracing system that is unique in the literature; and (iii) a schedule comparison was performed using the PSBS system and traditional bracing. The whole site was divided into four zones, and the excavation of each zone was carried out in three phases. The movement of piles, raker, waler, shore pile, capping beam, and the surrounding structure was monitored three-dimensionally. Moreover, the filed data was compared with the allowable limit of local code.

2. Case Study

2.1. Project Description

In this study, a 27-story five-star hotel with two basements is located in the Bangladeshi city of Khulna, with a basement space of 2133.6 m² and a ground floor area of roughly 37861.2 m². A 27-year-old brick technical school building is located on the project's eastern boundary, while a tin-shade residential building is on the project's northern boundary. The two-layer bracing system is introduced at the top of the basement slab, 5.8 m below the road level. The pump room, treated water tank, raw water tank, firewater tank, and wastewater treatment plant are below the basement level. The bottom of the excavation is 11.275 m from the basement level.

2.2. Supporting system

As a retaining wall system, where a 500 mm x 500 mm capping beam is provided on top of the shore pile to avoid trapping the shore pile, a 500 mm diameter and 15m~18m depth shore pile with a 100 mm gap between two shore piles are used as shown in Fig. 1. Additionally, sheet pile is introduced on the outer side of the shore pile.

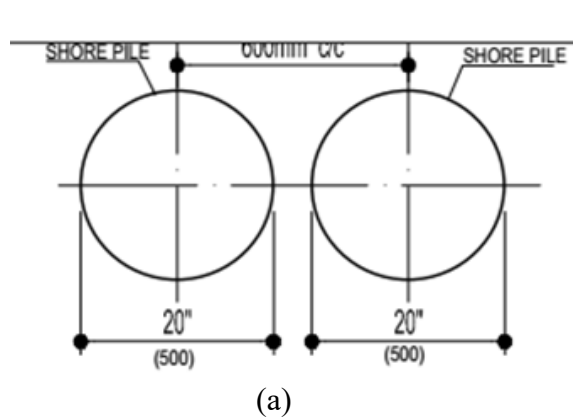


Fig. 1. (a) Setting out of the shored pile, (b) as-built shore pile location.

2.3. Bracing System

Three layers of I-beam with a 600 mm king post have been introduced for excavation. The first brace layer is at -2.2 m, the second is at -4.0 m, and the third is at -7.0 m below zero or road level.

2.4. Problem statement of the original design

The project is in a densely populated urban region, with public roads on the west and south sides. The eastern border of the project features a masonry technical school building constructed 27 years ago. It was found that there was a combination of very soft, soft, and organic soil in the subsurface. However, the project started to excavate according to the original plan without sheet piling. Eventually, water and soil penetrated the 100 mm gap between the shore piles. As

a result of the seepage of water and soil movement, the adjacent road, drain, and a portion of the tin-shade building were damaged. It was noticed that some king posts could not resist lateral forces from horizontal bracing [17]. It was almost impossible to excavate by overcoming all the obstacles. However, considering the local perspective, the project used an innovative low-cost excavation method known as the Pile Supported Bracing System (PSBS).

2.5. Sub Soil Conditions

This is the first instance in Khulna City, Bangladesh, to complete a double basement structure on soft soil. According to Table 1, the soil consists mainly of silt and clay, with just a tiny amount of fine sand present.

Table 1. Soil profile in terms of depth of the project location

Depth from EGL (m)	Soil type
0-6	Fine Sand
6-9	Very soft silty clay
9-12	Black organics
12-13.5	Clayey silt
15.5-26	Very soft to medium clayey SILT
26-29	Black decomposed
29-35	Medium stiff to clayey SILT
35-39.5	Gray medium-stiff to stiff silty CLAY
39.5-42.5	Gray medium-stiff clayey SILT
42.5-45.5	Gray stiff to very stiff silty CLAY
45.5-48.5	Brown very stiff silty CLAY
48.5-50	Brown stiff clayey SILT
50-60	Very dense silty SAND

3. Pile Supported Bracing Systems

An alternative pile-supported bracing systems (PSBS) was implemented to address the shortcomings of the initial construction project design. The PSBS method (Fig. 2) involves connecting (raker) steel I-beams to existing working/service piles to maintain the retaining wall structure during excavation. The PSBS approach is implemented by dividing the site into four phases, as indicated in Fig. 3.

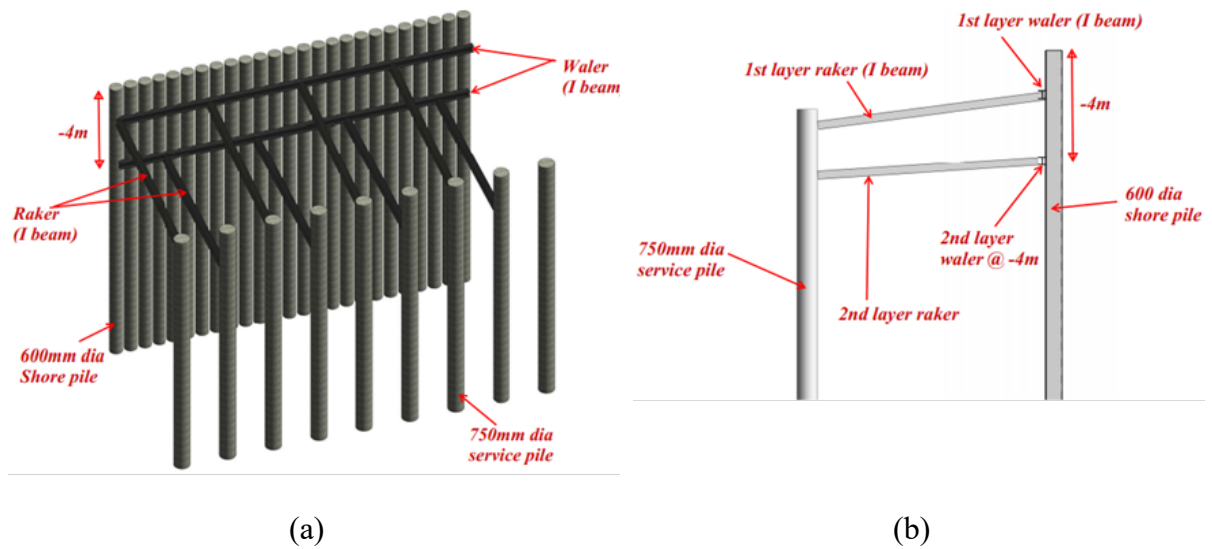


Fig. 2. (a) 3D view of PSBS method, (b) Typical section of PSBS

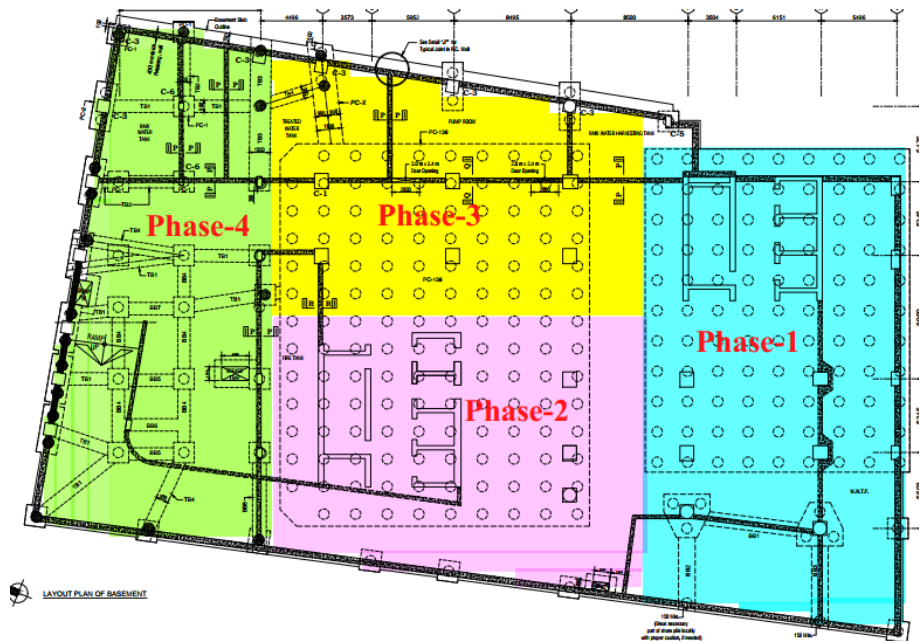


Fig. 3. Phases of basement construction

3.1. Sequences of Basement Construction

Step 1: Excavate -1m from the top of the capping beam.

Step 2: Install water beam onshore piles and pack the gap between water and shore pile to transfer uniform load.

Step 3: Install the raker (I-beam) with the first layer of water (I-beam) that is installed on onshore piles (Fig. 2).

Step 4: Further excavate up to 1.0m, and a 100mm thick skin wall (Fig. 4) is cast at the inner side of the shore pile on the same day to prevent water and soil slurry ingress.

- Step 5: Repeat steps 2 to 4 until - 4.0m of excavation.
- Step 6: Install the 2nd layer of the waler beam at 4.0 m levels (Fig. 2 and Fig. 4).
- Step 7: Install the raker (I-beam) with the 2nd layer of waler (Figs. 2 and 4).
- Step 8: Repeat steps 2 to 4 until the formation level of the basement slab.
- Step 9: Cast Phase-1 of the basement slab at 2–2.5 m from the shore pile.
- Step 10: Cast the first lift retaining wall 2 m high from the basement slab.
- Step 11: Remove the 2nd layer of waler and raker, followed by backfilling behind the shore piles.
- Step 12: Excavate for Phase-2 of the basement raft and followed by casting.
- Step 13: Transfer the raker from the working pile to the Phase-2 raft.
- Step 14: Excavate for Phase-3 of the raft.
- Step 15: Cast vertical elements from the basement to the semi-basement.
- Step 16: Cast semi-basement beam and slab
- Step 17: Cast vertical elements from the semi-basement to level-1
- Step 18: Cast level-1 beam and slab.
- Step 19: Completion of basement construction.



(a)



(b)

Fig. 4. (a) Reinforced concrete wall, (b) Application of the PSBS method.

4. Instrumentation

To reduce the risk of excavation, a total 20 prisms were installed on the cap of beam and adjacent school building to monitor 3-dimensional movement, with readings taken using a total station. Fig. 5(a) depicts the arrangement of the installed prism distributed in Phase-2 (T-01 to T-03), Phase-3 (T-04 to T-08) and Phase-4 (T-09 to T-12). The prism was also installed in the adjacent school building (B-01 to B-08). Figs. 5(b) and 5(c) show the installed prism on the school building and the cap of beam.

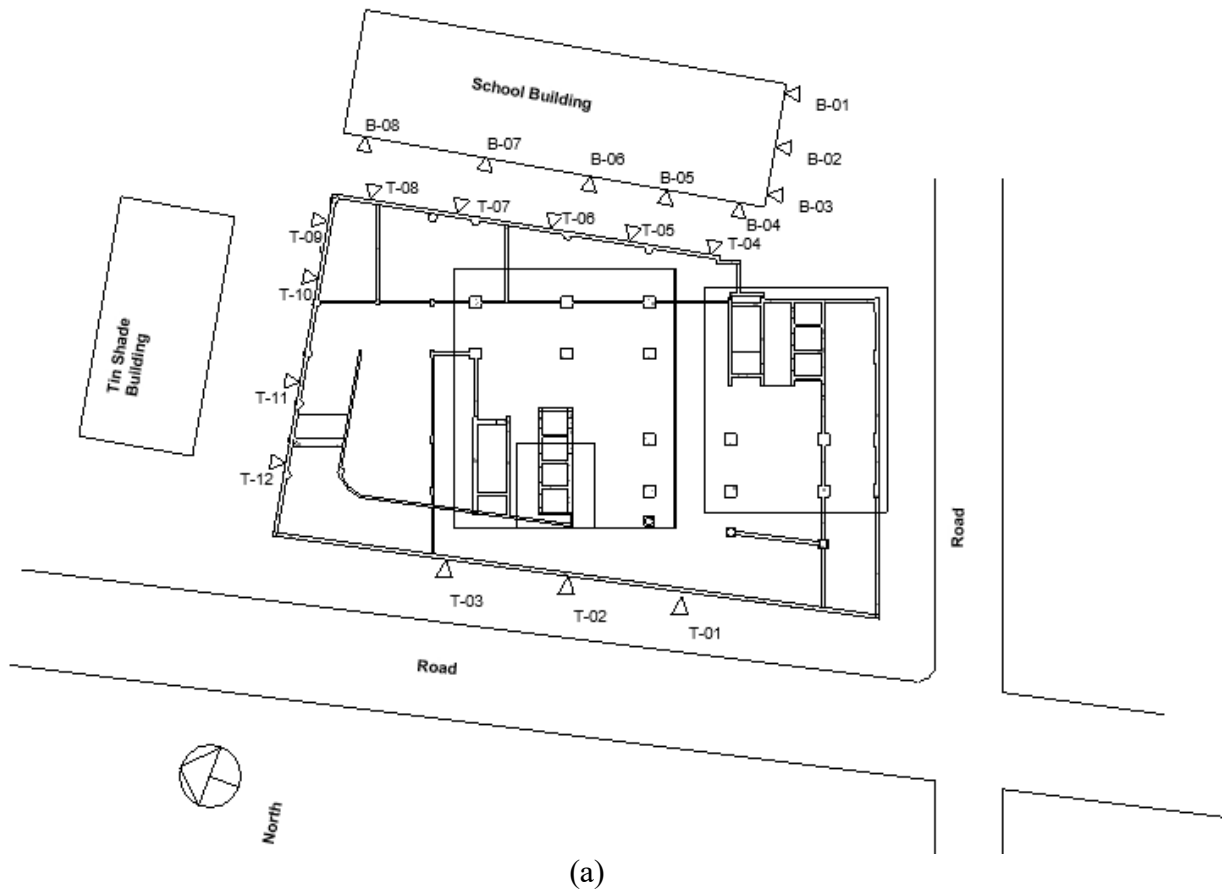
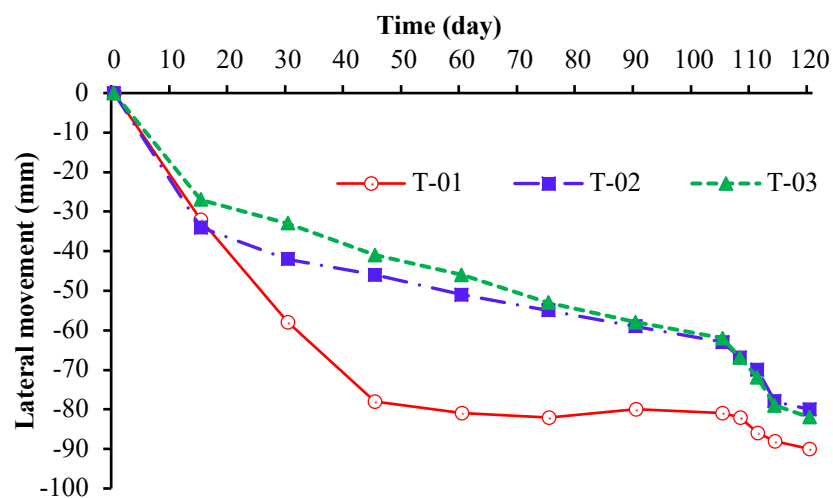


Fig. 5. (a) Prism layout plan, (b) Prism installed on the adjacent school building and (c) Prism installed on the capping beam

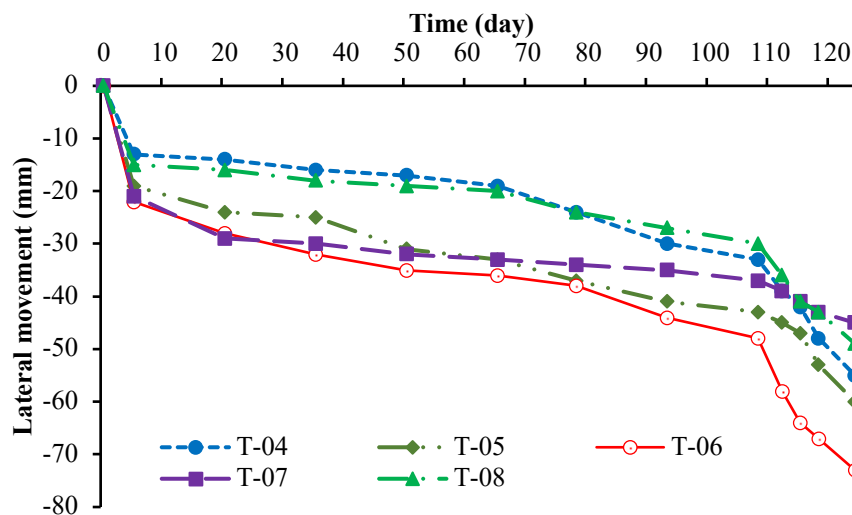
5. Field Performance of Pile-Supported Bracing Systems

5.1. Lateral Movement of Support System and Adjacent Building

Figs. 6(a), (b), and (c) illustrate the lateral movement of the shore pile retaining wall system during excavation for Phases-2, 3, and 4, respectively. A prism reading was taken during each phase of excavation to track the lateral movement of the support system. The lateral movement increases with the increase in the depth of excavation. Maximum capping beam movement was measured at 90 mm in the direction of excavation for Phase-2 and 73 mm and 55 mm for Phases-3 and 4, respectively. Due to additional excavation for the lift core, Phase-2 has a more significant movement than Phase-1. However, there is no considerable damage due to the excavation of the adjacent property. In compliance with the previous findings, if the ground movement is within a tolerable limit, there will be no or no damage to the surrounding property [18].



(a)



(b)

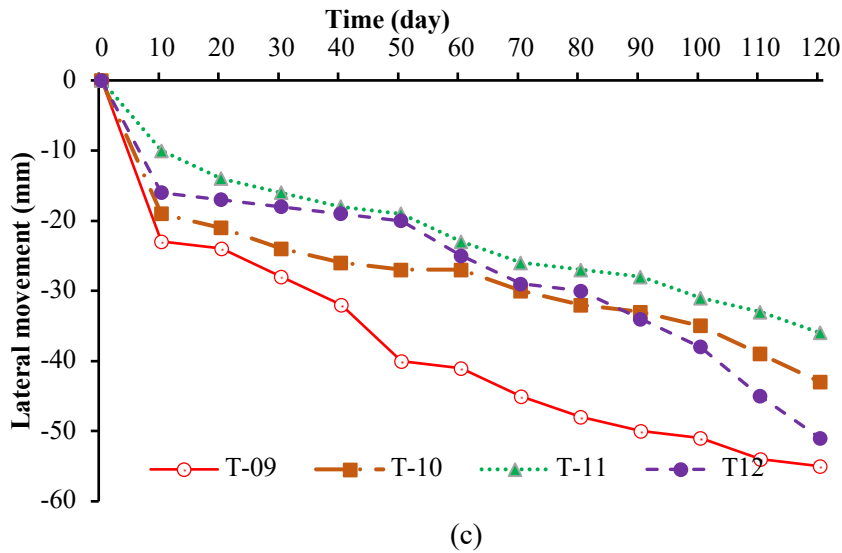


Fig. 6. Lateral movement of shore pile (a) Phase-2, (b) Phase-3, and (3) Phase-4.

To monitor the lateral movement of the adjacent existing property (i.e., a school building) due to deep excavation, a series of eight prisms (B-01 to B-08) have been fixed on the existing school building. As shown in Fig. 7, the maximum horizontal movement of the adjacent building due to excavation is observed at the location of prism B-08, with a magnitude of around 8mm. This is because prism B-08 is located very close to the excavation, and the depth of the excavation is relatively higher than in other locations. Additionally, it was observed that the minimum movement appeared at the locations of prisms B-04 and B-05 because the depth of excavation adjacent to them is relatively shallower. However, the 8mm lateral movement due to deep excavation is within the code tolerance (i.e., allowable 75mm).

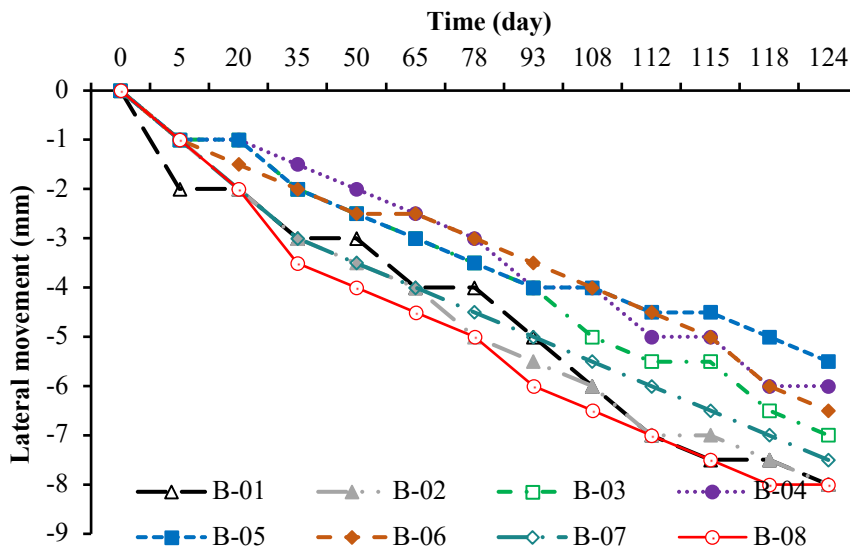
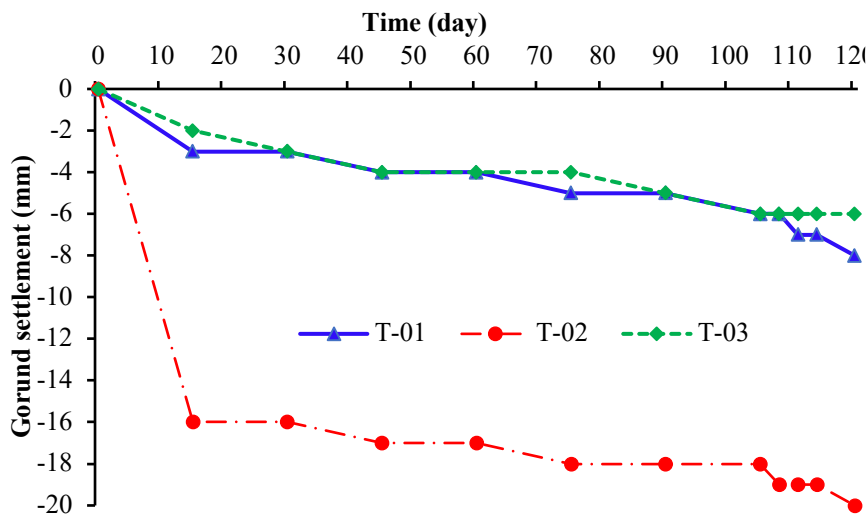


Fig. 7. Lateral movement of adjacent school building due to excavation

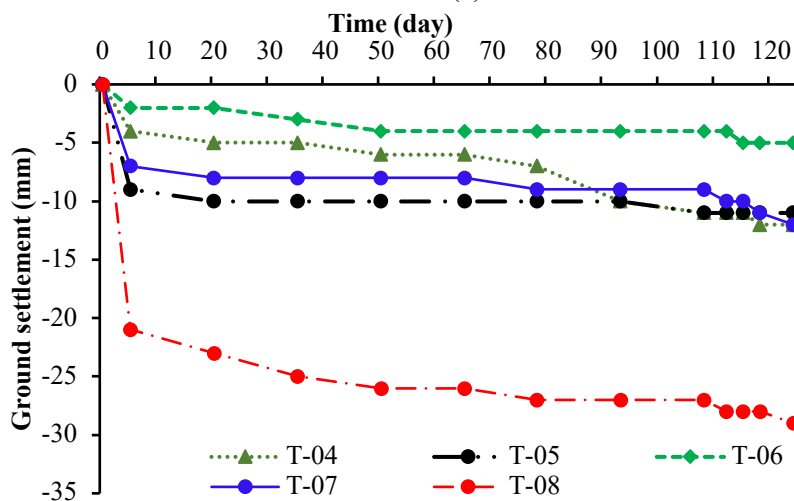
5.2. Settlement of Ground Surface

The degree of safety during excavation is contingent upon the surrounding ground settlement. A total of twelve prisms have been constructed along the boundaries of the project. Figs. 8 (a), (b), and (c) depict the extent of settlement observed during the excavation stages corresponding to Phases 2, 3, and 4, respectively. The reported average settlement for the prism T-02 during Phase-2 was 20 mm, but the prism T-08 demonstrated a maximum settlement of 29 mm during Phase-3. The prism T-12 demonstrates a maximum settlement magnitude of 39mm during Phase-4. However, the extent of the settlement was limited to 1.0m, excluding the capping beam. The main factor contributing to the settlement observed in Phase-4 of this study was the infiltration of soil slurry into the shore pile before the construction of the protective face of the wall. Prior to commencing any excavation, it is imperative to do a thorough risk assessment and implement appropriate precautionary measures. Nevertheless, the occurrence of ground settling during excavation is an inevitable hazard that has the potential to cause harm to the adjacent structure [19].

The adjacent school building has eight prisms (B-01 to B-08) installed to monitor movement during excavation. The measured prism reading is displayed in Fig. 9, and for the B-06 prism, the maximum ground settlement was 9 mm. Every curve was also found to move vertically, which may be the result of vibrations from excavation.



(a)



(b)

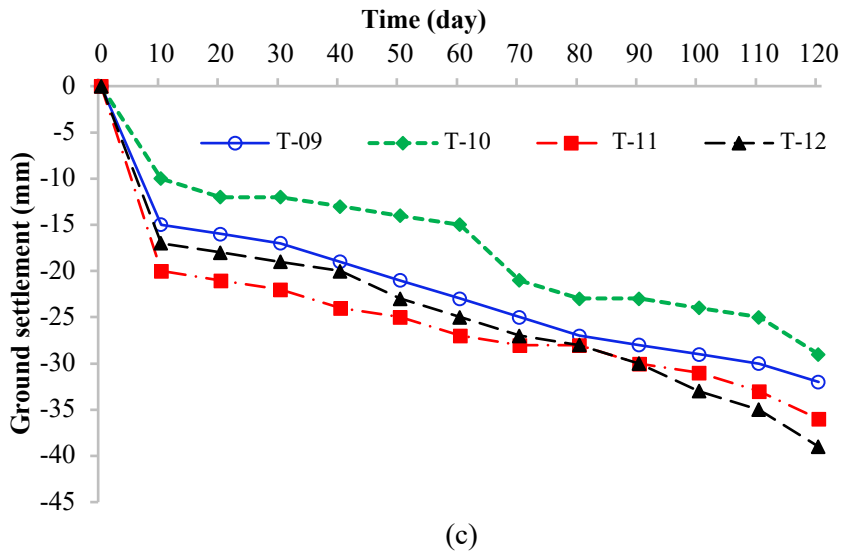


Fig. 8. Adjacent ground surface settlement due to excavation (a) Phase-2, (b) Phase-3, and (c) Phase-4

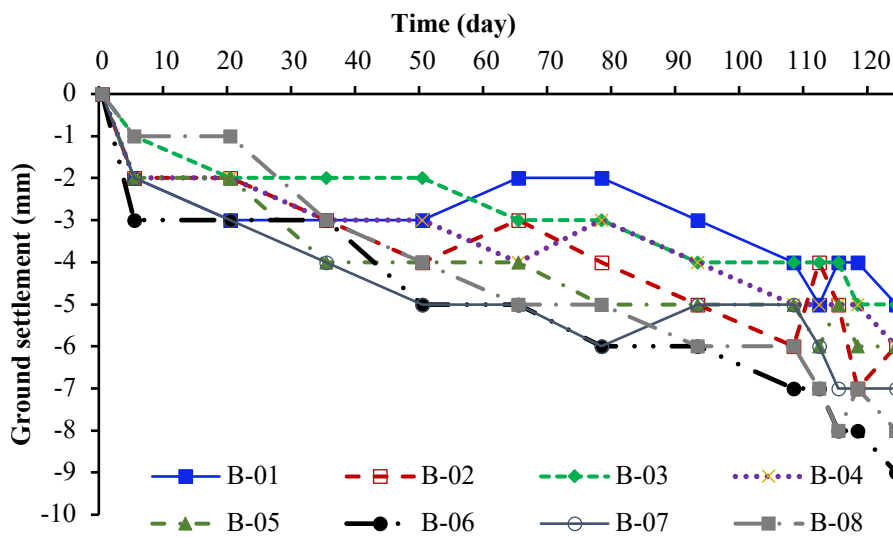
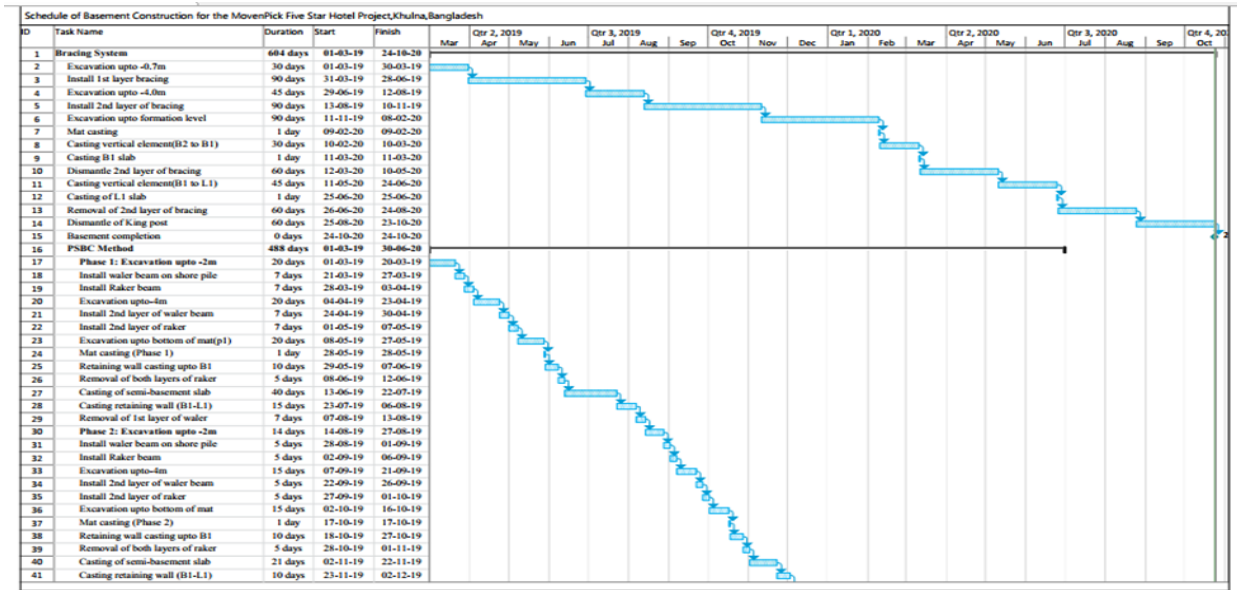


Fig. 9. Ground settlement of adjacent school building due to excavation

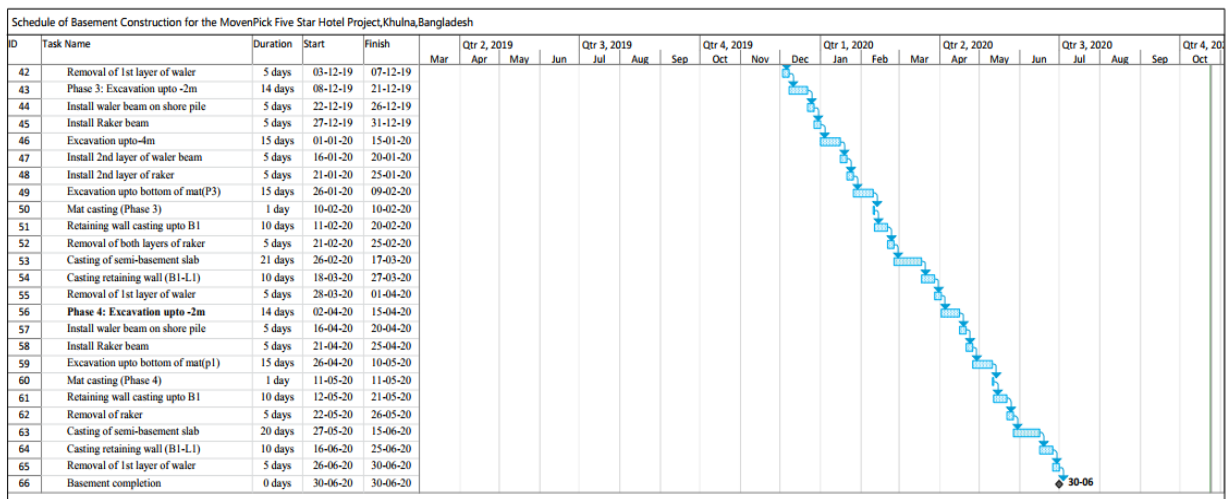
5.3. Schedule Comparison

Fig. 10 illustrates the duration necessary to complete basement construction while employing the original internal bracing system and the PSBS. Based on the findings of the PSBS, it is observed that the duration for basement construction spans a period of 331 days, but the installation of the internal bracing system requires a timeframe of 603 days. To clarify, the PSBS system reduces time by 272 days compared to the internal bracing method. Research has

revealed that the elimination of the three-layer bracing system is a significant determinant in the time-saving capabilities of the PSBS system. The utilization of internal bracing in



(a)



(b)

Fig. 10. Comparison of schedule between (a) bracing and (b) PSBS system

construction projects has resulted in lower productivity levels compared to the implementation of the proprietary PSBS system. This discrepancy can be attributed to the increased number of preparatory operations required prior to excavation when employing internal bracing.

5.4. Comparison of Cost

The PSBS approach is a cost-effective solution, exhibiting a significant 50% decrease in construction prices compared to an internal bracing system, as depicted in Fig. 11. Significantly, the PSBS approach eliminates the need for a king post, optimizing the construction process and reducing the material necessary. A comparatively low steel I-beam is adequate for attaining structural stability, leading to cost reductions and enhanced efficiency.

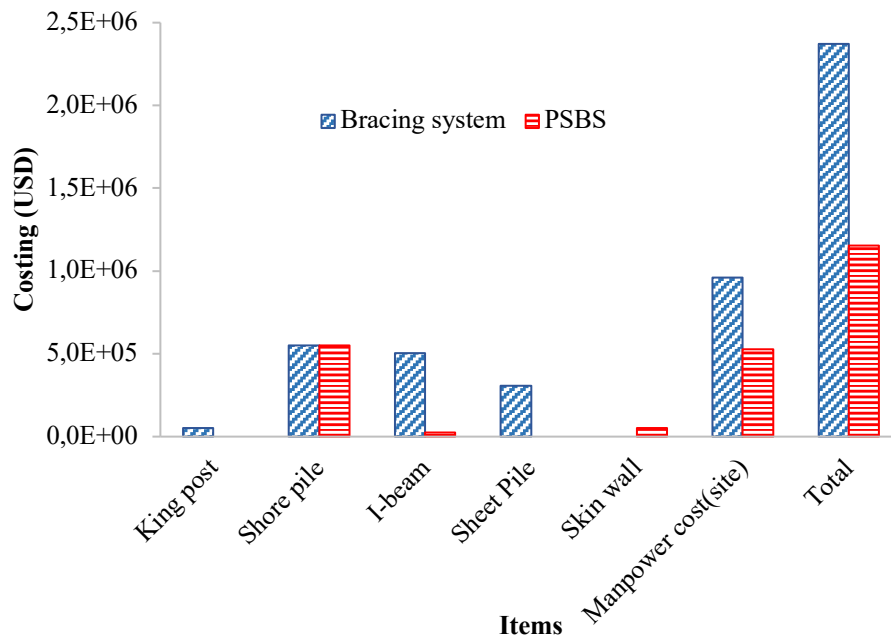


Fig. 11. Comparison of cost between bracing and PSBS

On the other hand, the utilization of the internal bracing technique presents the benefit of obviating the need for a reinforced concrete wall, thereby resolving particular construction considerations. It is important to note that in the original design, supports for sheet piles were built into the shore pile from the outside. This gives the structure more flexibility to adapt to site conditions and building needs. Implementing the PSBS method in a planned manner not only results in significant cost reductions but also improves the general flexibility and durability of the building methodology.

6. Conclusions

Deep excavations conducted in urban environments pose significant risks due to the substantial settlement of the surrounding soil. This settlement can result in the failure of retaining wall systems, ultimately leading to the collapse of adjacent properties. The inclusion of a retaining wall and bracing system is crucial in the successful execution of deep excavations for a basement construction endeavour. The total station was monitored three-dimensionally, like the adjacent school building, ground surface settlement, and lateral movement of supporting systems. The implementation of the PSBS was undertaken in order to effectively resolve the challenges associated with the first internal bracing strategy. The two-level basement of a 27-storied five-star hotel complex was completed using the unique PSBS technology. The use of the PSBS methodology in constructing a basement resulted in a reduction of 272 days in the project timeline and a 50% decrease in costs compared to the implementation of an internal bracing solution. The maximum lateral displacement of the supporting shore pile structure is measured to be 90 mm, but the maximum settlement observed on the ground surface is recorded at 39 mm. The primary cause of this type of settlement was the infiltration of soil slurry into the shore pile before constructing the surface wall. The lateral displacement of the support system, adjacent building, and ground settlement were found to be within the permissible limits. The present study employs a cost-effective and innovative pile-supported bracing system (PSBS) for the purpose of deep excavation in the building. The PSBS excavation method was

developed and subsequently utilised for constructing a two-level basement using the bottom-up technique. The proposed PSBS approach may be employed for the construction of both deep and shallow basements.

Author Contributions

Md. Alhaz Uddin: Performed the analysis, Wrote the paper, Modified the paper.

Mizanoor Rahman: Conceived and designed the analysis, Collected the data, Contributed data or analysis tools.

References

- [1] Zhang, J.F., Chen, J.J. Wang, and Zhu, Y.F., Prediction of tunnel displacement induced by adjacent excavation in soft soil, *Tunnelling and Underground Space Technology*, 36, 24-33, 2013.
- [2] Li, S. and Lu, W., Characteristics of ground surface settlement associated with deep excavation in Beijing city, *2020 International Conference on Urban Engineering and Management Science (ICUEMS)*, 159-163, 2020.
- [3] Konai, S., Sengupta, A., and Deb, K., Effect of excavation depths on ground surface settlement for embedded cantilever retaining structure due to seismic loading, *Procedia engineering*, 199, 2342-2347, 2017.
- [4] Hsiung, B.C.B. and Dao, S.D., Prediction of ground surface settlements caused by deep excavations in sands, *Geotechnical Engineering*, 46(3), 111-118, 2015.
- [5] Godavarthi, V.R., Mallavalli, D., Peddi, R., Katragadda, N., and Mulpuru, P., Contiguous pile wall as a deep excavation supporting system, *Leonardo Electronic Journal of Practices and Technologies*, 19, 144-160, 2011.
- [6] Blackburn, J.T. and Finno, R.J., Three-dimensional responses observed in an internally braced excavation in soft clay, *Journal of Geotechnical and Geoenvironmental Engineering*, 133(11), 1364-1373, 2007.
- [7] Finno, R.J., Bryson, S., and Calvello, M., Performance of a stiff support system in soft clay, *Journal of Geotechnical and Geoenvironmental Engineering*, 128(8), 660-671, 2002.
- [8] Hashash, Y.M., and Whittle, A.J., Mechanisms of load transfer and arching for braced excavations in clay, *Journal of geotechnical and geoenvironmental engineering*, 128(3), 187-197, 2002.
- [9] Hsieh, P.G., and Ou, C.Y., Shape of ground surface settlement profiles caused by excavation, *Canadian geotechnical journal*, 35(6), 1004-1017, 1998.
- [10] Hudson, M.B., Cefali, D.A., Lew, M., and Crow, M.R., Design of a Deep Tied-Back Excavation Adjacent to the Los Angeles Metro Red Line Subway, *Geotechnical and Structural Engineering Congress 2016*, 537-550, 2016.
- [11] Liao H., and Hsieh, P., Tied-back excavations in alluvial soil of Taipei, *Journal of geotechnical and geoenvironmental engineering*, 128(5), 435-441, 2002.
- [12] Xiao, H., Zhou, S., and Sun, Y., Wall deflection and ground surface settlement due to excavation width and foundation pit classification, *KSCE Journal of Civil Engineering*, 23, 1537-1547, 2019.
- [13] Kung, G.T.C., Comparison of excavation-induced wall deflection using top-down and bottom-up construction methods in Taipei silty clay, *Computers and Geotechnics*, 36(3), 373-385, 2009.

- [14] Li, H., Liu, S., and Tong, L., Evaluation of lateral response of single piles to adjacent excavation using data from cone penetration tests, *Canadian Geotechnical Journal*, 56(2), 236-248, 2019.
- [15] Zhang, C., Huang, M., and Liang, F., Lateral responses of piles due to excavation-induced soil movements, *Geotechnical Aspects of Underground Construction in Soft Ground: CRC Press*, 865-872, 2008.
- [16] Wang, J., Xu, Z., and Wang, W., Wall and ground movements due to deep excavations in Shanghai soft soils, *Journal of Geotechnical and Geoenvironmental Engineering*, 136(7), 985-994, 2010.
- [17] El Sawwaf, M., and Nazir, A.K., The effect of deep excavation-induced lateral soil movements on the behavior of strip footing supported on reinforced sand, *Journal of Advanced Research*, 3(4), 337-344, 2012.
- [18] Hsieh, H.S., Wang, C.C., and Ou, C.Y., Use of jet grouting to limit diaphragm wall displacement of a deep excavation, *Journal of geotechnical and geoenvironmental engineering*, 129(2), 146-157, 2003.
- [19] Clough, G.W., Construction induced movements of in situ walls, *Design and performance of earth retaining structures*, 439-470, 1990.




Early Diagnoses of Acute Coroner Syndrome Based on Machine Learning Model

Umut Utku Tiryaki ^a, Gul Karaduman ^{b*}, Sare Nur Cuhadar ^c, Ahmet Uyanik ^d, Habibe Durmaz ^e

^{a,c,e} Karamanoğlu Mehmetbey University, Department of Electrical and Electronics Engineering, Karaman, Türkiye

^{b*} Karamanoğlu Mehmetbey University, Vocational School of Health Services, Karaman, Türkiye
^d Konya Meram State Hospital, Konya, Türkiye

✉ : gulk@bu.edu ^{b*}, durmazgul@gmail.com ^c,  : 0009-0000-5028-0782 ^a, 0000-0002-2776-759X ^{b*}, 0000-0003-4461-877X ^c, 0000-0001-5037-1019 ^d, 0000-0002-5929-861X ^e

Received: 27.10.2023, Revised: 05.01.2024, Accepted: 25.01.2024

Abstract

Cardiovascular diseases are a leading global cause of death, particularly in low to middle-income countries. Early and accurate diagnosis of Acute Coronary Syndrome (ACS) is vital, but limited access to healthcare hinders effective management. This study utilized machine learning to develop mathematical models for ACS risk detection. Data from 249 individuals with ACS or suspected heart disease were used to construct twelve models with different parameters and classifiers. Performance indicators, including accuracy, Matthews correlation coefficient, and precision, were employed for evaluation. The Random Forest classifier demonstrated superior performance, achieving 90.45% accuracy for internal validation and 86% for external validation. Critical criteria for ACS diagnosis were CK-MB, age, coronary artery disease, and Troponin T value. The models developed in this study significantly prevent potential deaths via rapid intervention and reduce healthcare expenditures by minimizing unnecessary human resources and repeat tests.

Keywords: Cardiovascular diseases; acute coronary syndrome; heart attack; machine learning; model performance.

1. Introduction

Cardiovascular diseases (CVDs) encompass conditions that cause damage to the heart and blood vessels, including cerebrovascular, coronary heart, and rheumatic heart diseases. The World Health Organization (WHO) identifies CVDs as the leading global cause of mortality [1], presenting a significant public health challenge. A 2016 study on the Global Burden of Non-Communicable Diseases reveals that 40% of non-communicable diseases in women and 50% in men can be attributed to cardiovascular and related diseases. In contrast, only 20% of female and 24% of male patients experience cardiovascular diseases alone [2].

Acute Coronary Syndrome (ACS), a specific type of cardiovascular disease, refers to heart tissue damage resulting from blockages in the coronary arteries, commonly known as a heart attack. ACS accounts for 4 out of 5 deaths related to CVDs, with 1 out of 3 deaths occurring in individuals below 70 years of age [3]. Chest pain serves as the prominent symptom of cardiovascular diseases and ACS, and it is challenging to distinguish between common chest pain and suspected ACS. Despite advances in treatment, readmission rates for ACS patients remain elevated [4].

Cardiovascular diseases (CVDs) claim the lives of approximately 18 million individuals annually, making them the leading cause of global mortality in 2019. Most of these deaths occur in middle- and low-income countries, including Central Asia, Eastern Europe, and other low-



income regions [5]. The economic impact of CVDs is substantial, with significant costs reported in various countries, such as Serbia, the Fiji Islands, sub-Saharan Africa, Turkey, Brazil, and India [6-11].

To ensure early diagnosis and treatment for individuals at high risk of CVDs, universal access to primary healthcare services is imperative within the next 25 years. Currently, many people in low-income countries need access to such services [12]. Artificial intelligence algorithms offer a promising solution by expanding primary healthcare and enabling early detection of ACS and other diseases such as COVID-19 without the need for costly tests or excessive human resources [13-15]. Mathematical models employing machine learning techniques have been developed to identify ACS risk using data from individuals who experienced ACS and those with suspected heart conditions but no ACS diagnosis.

Our research underscores the notable success achieved in early Acute Coronary Syndrome (ACS) diagnosis through the implementation of sophisticated mathematical machine-learning models. The overarching aim is to prevent avoidable deaths by facilitating timely intervention, and curbing unnecessary resource utilization, and redundant testing, thereby resulting in a tangible reduction in healthcare expenditures. Significantly, our model equips healthcare professionals with a streamlined approach to promptly assess patients with suspected ACS, eliminating the need for extensive and costly diagnostic procedures.

A groundbreaking aspect of our study is the introduction of an innovative approach that harnesses artificial intelligence algorithms for the early detection of ACS. Through the integration of intricate mathematical models and advanced machine learning techniques, our research endeavors to enhance early diagnosis of mortal diseases such as ACS, COVID-19, ebola virus, etc, mitigating the necessity for costly tests a pivotal advancement in optimizing healthcare resource allocation [13-15].

Central to our contributions is the development and validation of mathematical machine-learning models specifically tailored for the early diagnosis of ACS. Emphasizing the model's remarkable success rates, we highlight its capacity to empower healthcare practitioners to efficiently evaluate patients presenting with suspected ACS, leading to more targeted and cost-effective interventions.

In positioning our proposed model, we assert its pivotal role in averting preventable deaths through timely interventions, curbing unwarranted resource consumption, and ultimately reducing overall healthcare expenditures. This strategic alignment aligns with broader healthcare objectives, including the enhancement of efficiency, cost reduction, and improvement of patient outcomes.

2. Material and Methods

To create predictive models for the early detection of acute coroner syndrome, (Waikato Environment for Knowledge Analysis (WEKA) (<https://www.cs.waikato.ac.nz/ml/weka>) was utilized in this study [35]. The development process for these models is outlined in Figure 1. The initial step involved preprocessing the dataset, which included removing noisy data, normalizing the dataset, and determining the applicable range. Subsequently, the dataset was divided into a training set (80% of the data) and a test set (20% of the data). Various techniques were employed to identify the most suitable parameters for constructing accurate predictive machine-learning models. Twelve machine learning modeling algorithms were utilized to diagnose obesity based on blood analysis, and their performance was evaluated using measures derived from the confusion matrix for internal and external validation.

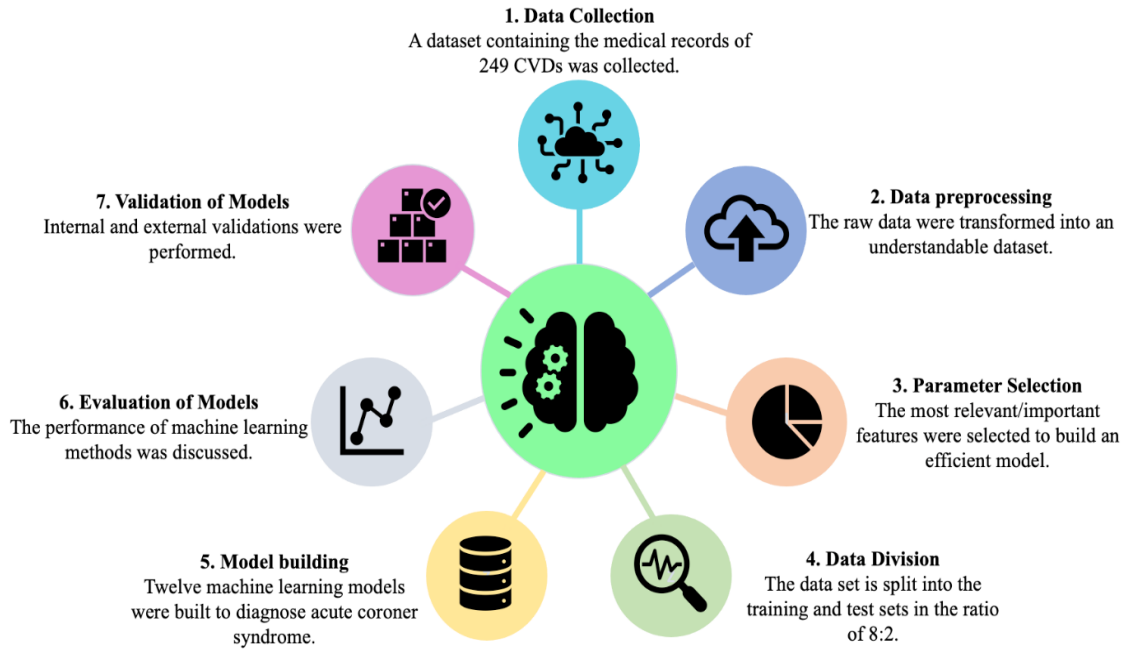


Fig. 1. The model development process for early diagnoses of acute coroner syndrome.

2.1. Details of the dataset

The study comprised 249 participants, some experiencing ST-elevation myocardial infarction or myocardial infarction without ST elevation, collectively called ACS. Among the participants, 191 individuals had a history of heart attack, while the remaining 58 did not exhibit signs of ACS. Detailed patient information, including age, gender, blood test results, and medical conditions like smoking, hypertension, and diabetes, which contribute to ACS risk, can be found in Table 1. The dataset provides further insights and is presented in Table 1.

Table 1. Features and risk factors of acute coronary syndrome

Serial Number	Group	Feature Names	Features Descriptions
1	Patient record data	Age	Age in years
2	Patient record data	Sex	1 = female; 2 = male
3	Patient record data	Smoke	1 = smoker; 0 = non smoker
4	Patient record data	Hypertension	History of hypertension
5	Patient record data	Diabetes	1 = history of diabetes; 0 = no such history
6	Patient record data	Troponin T	Troponin T value in blood test
7	Patient record data	CK-MB	CK-MB value in blood test
8	Patient record data	Hyperlipidemia	1 = high cholestrol; 0 = no high cholestrol
9	Patient record data	Heart failure	1 = History of heart failure; 0 = no such history
10	Patient record data	Coronary artery disease	1 = History of having a previous heart attack; 0 = no such history
11	Patient record data	Coronary Artery Graft	1 = History of having coronary angiography; 0 = no such history
12	Patient record data	Coronary by-pass	1 = History of having coronary artery by-pass surgery; 0 = no such history
13	Patient record data	Chronic renal failure	1 = History of chronic renal failure; 0 = no such history

The details of the dataset used in the study are as follows:

- a. *Patient's age*: Age is a significant risk factor for coronary artery disease, and the risk of acute coronary syndrome (ACS) and mortality increases steadily. After accounting for other risk factors, the risk of ACS-related death rises by two to three times per decade [16]. Most ACS-related deaths happen in individuals aged 65 or older [17], with over half of these deaths occurring in those aged 70 or above.
- b. *Gender*: Research has indicated that being male is an independent risk factor for coronary artery disease [18]. On average, men develop coronary artery disease 7-10 years earlier than women [19]. This disparity is attributed to the protective influence of estrogen, which may explain the heightened risk in women who undergo premature menopause [20].
- c. *Smoke*: Smoking is a substantial and separate predictor for the onset of coronary artery disease, and quitting smoking reduces the risk of acute coronary syndrome (ACS) [21]. Smoking elevates blood pressure and heart rate, resulting in heightened peripheral vascular resistance and the release of catecholamines. It diminishes flow-mediated dilation in the coronary artery, promotes blood clot formation, and lowers HDL cholesterol levels. Moreover, smoking directly damages the endothelial lining, contributing to the development of atherosclerosis [17].
- d. *Hypertension*: Numerous observational studies have established a robust association between elevated blood pressure and the likelihood of coronary artery disease [18]. Each increment of 20 mm/Hg in systolic blood pressure or 10 mm/Hg in diastolic blood pressure doubles the risk of ACS-related mortality and stroke [22].
- e. *Diabetes*: Both type 1 and type 2 diabetes are linked to an increased risk of acute coronary syndrome (ACS) [23]. Individuals with diabetes who have a history of ACS face a greater risk of mortality compared to those without diabetes. Diabetes amplifies the risk of ACS by two to four times and, when combined with high cholesterol, serves as a significant predictor of coronary disease. Approximately 80% of patients with diabetes develop coronary atherosclerosis [21, 23].
- f. *Troponin T*: Cardiac troponins play a crucial role in regulating the calcium-dependent interaction between actin and myosin in the heart [24]. Numerous studies have demonstrated a correlation between troponin levels and the risk of mortality in acute coronary syndrome (ACS) [25]. Troponin T, primarily present in the myocardium, exhibits high clinical sensitivity, enabling the detection of even minor increases [26, 27].
- g. *CK-MB*: Creatine is a vital protein present in muscle cells, with notable concentrations in skeletal and cardiac muscles. In conditions that compromise muscle cell integrity, creatine kinase can be released into the bloodstream, leading to a substantial elevation in blood creatine kinase levels [28]. Among the three isoenzymes of creatine kinase, CK-MB was incorporated into the model due to its predominant occurrence in cardiac muscle cells and its tendency to increase in the blood during ischemic heart disease.
- h. *Hyperlipidemia*: Hyperlipidemia denotes elevated levels of fats in the bloodstream. Numerous studies have established a robust association between low-density lipoprotein (LDL) cholesterol and the progression of atherosclerotic vascular disease. Additionally, reduced levels of high-density lipoprotein (HDL) cholesterol serve as a risk factor for heightened coronary artery disease risk [29].
- i. *Congestive heart failure*: Heart failure can arise due to multiple factors, with the most prevalent causes being ischemic heart disease and acute coronary syndrome (ACS) induced

by atherosclerotic vascular disease. Malnutrition and myocardial necrosis resulting from ACS can result in impaired contraction function of the heart muscle [30].

- j. *Coronary artery disease*: The coronary arteries play a critical role in providing the heart with essential oxygen and nutrients. Diseases affecting these arteries have a direct impact on heart function and efficiency. The buildup of substances, primarily cholesterol, results in the narrowing and blockage of the coronary arteries, giving rise to atheromatous plaques that progressively restrict the vessel's lumen. This narrowing hampers blood flow to the heart, leading to issues associated with coronary artery disease, often presenting as acute coronary syndrome (ACS) [31].
- k. *Coronary artery imaging and coronary bypass*: For patients experiencing acute coronary syndrome (ACS), coronary angiography and angioplasty are employed to reinstate blood flow in the coronary artery obstructed by atheromatous plaque. In instances where coronary angioplasty fails to achieve revascularization, coronary bypass surgery is the preferred approach. This surgical intervention enhances symptoms and enhances the disease prognosis, leading to improved outcomes [32].
- l. *Chronic kidney disease*: Chronic kidney disease is a condition marked by a decline in kidney function, resulting in the loss of nephrons and a gradual decrease in glomerular filtration rate (GFR) over time [33]. While chronic kidney disease itself is not a direct risk factor for acute coronary syndrome (ACS), it can lead to false-positive Troponin T levels in individuals with this condition [26].

2.2. Data preprocessing

The preprocessing and data cleaning stages are crucial for the success and accuracy of machine learning modeling. Some collected data may require correction or may be missing due to noise [34]. During preprocessing, the noise was removed from the data set. Rows containing invalid data were deleted, and missing values were updated by taking the average of corresponding data groups. Duplicates were also removed. Additionally, names and last names were removed to avoid possible confusion. Normalization was applied by rescaling data between 0 and 1 to improve accuracy.

2.3. Data Division

The data was split into two sets: 80% for training and 20% for testing. The training and test data were independently separated to avoid a false accuracy rate, which can occur when using exact data for training and testing.

2.4. Parameter Selection

Real-time intrusion detection is nearly impossible due to the large amount of data flowing over the network. Feature selection can reduce the calculation time and complexity of the model. Feature selection is selecting the relevant and vital features by removing the most irrelevant and redundant features from the dataset to build an effective and efficient model. Two attribute selection techniques were used in this study. The CfsSubsetEval evaluator, combined with the Best First search method, is a correlation-based attribute selection method that determines the prediction power of each attribute. The CorrelationAttributeEval evaluator works with the Ranker search method and selects the attributes that will create the best models based on Pearson's correlation logic. Feature selection reduces calculation time and model complexity by selecting relevant and vital features and removing irrelevant and redundant ones from the dataset.

2.5. Algorithms

In this study, four classifiers, namely Bayes Net, Logistic, IBk, and Random Forest were chosen and applied to the dataset. The selection of Bayes Net, Logistic Regression, IBk (k-Nearest Neighbors), and Random Forest classifiers was based on a strategic consideration of the dataset's characteristics. Bayes Net and Logistic Regression were chosen for their interpretability, IBk for its effectiveness in handling diverse data distributions, and Random Forest for its robustness and ability to capture complex relationships. These choices aim to provide a comprehensive evaluation, ensuring a balanced exploration of methodological approaches in addressing the study objectives. A summary of these classifiers is provided below.

2.5.1. Bayes Net

The Bayes Net classifier is a statistical classifier that uses multiple search algorithms and quality measures based on the Bayes network classifier [36]. It is based on Bayes' Theorem [37], which calculates the conditional probability of E_j , given A, from the probabilities of E_1, E_2, \dots, E_k and the conditional probabilities of A was given E_i , $i=1,2, \dots, k$ is calculated by

$$P(E_j|A) = \frac{P(A \cap E_j)}{P(A)} = \frac{P(E_j)P(A|E_j)}{\sum_{i=1}^k P(E_i)P(A|E_i)}. \quad (1)$$

2.5.2. Logistic

The Logistic regression classifier is a popular classification method with extensive usage [38]. It is easy to implement and has exhibited excellent performance across various issues, including spam prediction. The classification model is appropriate for estimating discrete probabilities, such as outcomes in the form of yes, no, win, or lose. Additionally, this classifier is straightforward to execute and has demonstrated competent performance across various issues [39].

2.5.3. IBk

The IBk algorithm predicts the outcome of a test pattern in real-time without requiring the construction of a model during classification. To make predictions, the algorithm measures the distance between each test sample and k neighboring instances in the training data, selecting a particular distance measure to make an estimation. The classification function then incorporates the results obtained and the similarity function to determine which instances to include in the description concept [40].

2.5.4. Random forest

The random forest classifier combines decision trees to increase the classifier value. The algorithm generates multiple decision trees during classification and combines them to form a decision forest. Each classifier is created by randomly sampling a vector from the input [41]. The algorithm replaces the original sets to form training sets, and a new subset and random attribute selection create the tree. The node is then split using the best splitting on the randomly chosen attributes [42].

2.6.Evaluation of the Models

In this section, the metrics utilized in this study are described. These metrics are based on the four values (TP, FN, TN, FP) from the confusion matrix [56, 57]. As shown in Figure 2, the confusion matrix has labels for both positive and negative classes in both actual and predicted outcomes. When data has a positive label in the actual class and a positive label in the predicted class, it is considered a "True Positive (TP)," while a positive label in the predicted class but a negative label in the actual class is considered a "False Positive (FP)." Conversely, when data has a negative label in the actual class and a positive label in the predicted class, it is considered a "False Negative (FN)," while a negative label in both actual and predicted classes is considered a "True Negative (TN)."

		Actual Class	
		Positive	Negative
Predicted Class	Positive	TP	FP
	Negative	FN	TN

Fig. 2. Confusion matrix for binary classification

(a) Precision refers to the ratio of the truly positive or negative results to the total number of results.

$$\text{Precision} = \frac{\text{TN}}{\text{TN} + \text{FP}} \quad (2)$$

(b) Recall is the ratio of the data that a machine learning model correctly identifies as belonging to a class of interest.

$$\text{Recall} = \frac{\text{TP}}{\text{TP} + \text{FN}} \quad (3)$$

(c) MCC evaluates the correlation between actual data and the data predicted by the model.

$$\text{MCC} = \frac{\text{TP} \times \text{TN} - \text{FP} \times \text{FN}}{\sqrt{(\text{TP} + \text{FP})(\text{TP} + \text{FN})(\text{TN} + \text{FP})(\text{TN} + \text{FN})}} \quad (4)$$

(d) ROC Area: It is one of the most critical metrics for machine learning models. It shows the false positive and true positive rates, providing information about the model's overall performance.

(e) Accuracy: The Accuracy value is calculated as the ratio of correctly predicted values to the total dataset in the model.

$$\text{Accuracy} = \frac{\text{TP} + \text{TN}}{\text{TP} + \text{FP} + \text{TN} + \text{FN}} \quad (5)$$

(f) Kappa statistic obtains a value between 0 and 1 in the calculation. The statistics obtained between 0.00-0.20 are low, 0.20-0.40 are below average, 0.40-0.60 are average, 0.60-0.80 are strong, and 0.80-1.00 are excellent [43]. The kappa value is calculated as follows:

$$\text{Kappa statistic} = \frac{\text{observed aggrement} - \text{expected aggrement}}{1 - \text{expected aggrement}} \quad (6)$$

2.7. Validation of the Models

Validation is a crucial statistical resampling technique that plays a pivotal role in objectively and accurately assess the performance of a machine learning model when applied to unseen data. We conducted internal and external validations to ensure a comprehensive and unbiased evaluation of the methods employed in our modeling process. These validations serve as robust and reliable mechanisms to gauge the effectiveness and reliability of our chosen approaches, enabling us to obtain a more thorough understanding of the model's performance and its potential for generalization to new, unseen data. By employing these validation techniques, we aim to minimize any potential biases or overfitting issues, allowing us to confidently ascertain the true efficacy of our machine learning methods and their suitability for accurately diagnosing obesity based on the parameters derived from blood test results.

3. Results

In our study, we embarked on the development of a diverse set of twelve machine learning models, which were created by employing a combination of four distinct classification algorithms and three feature selection options. This approach allowed us to explore various avenues and harness the potential of different techniques to enhance the predictability and reliability of our models. To comprehensively evaluate the performance and effectiveness of these models, we conducted both internal and external validations, each serving a unique purpose in assessing their capabilities.

Internal validation, a crucial component of our evaluation framework, involved the utilization of a 10-fold cross-validation technique. This technique provided a robust and objective means of gauging the models' performance by partitioning the available data into ten equally sized subsets. By iterative training and evaluating the models on different combinations of training and validation sets, we were able to obtain a comprehensive understanding of their generalization ability and reliability in different scenarios.

Furthermore, external validation was conducted to assess the predictive power of the models on unseen data. This validation process involved evaluating the performance of the trained models on a dedicated test set, which was kept completely separate from the training data. By subjecting the models to this rigorous evaluation on an independent dataset, we were able to gauge their real-world applicability and assess their ability to accurately predict obesity based on the parameters derived from blood test results.

Through this extensive and rigorous validation process, we aimed to ensure that our machine learning models not only demonstrated strong performance during internal validation but also

exhibited a high degree of reliability and predictive capability when confronted with new, unseen data. By adopting these comprehensive validation procedures, we gained confidence in the efficacy and generalizability of our models, enabling us to make informed decisions about their suitability for diagnosing obesity based on blood analysis.

3.1. Internal Validation Performance

Among the various machine learning models and feature selection techniques evaluated in our study, the Random Forest classifier with CfsSubsetEval feature selection emerged as the top-performing model in terms of accuracy. It achieved an impressive accuracy rate of 90.4523%, accompanied by notable metrics such as an MCC (Matthews Correlation Coefficient) of 0.726, ROC (Receiver Operating Characteristic) of 0.942, Precision of 0.903, Recall of 0.905, and Kappa Statistic of 0.7251. These results highlight the model's ability to make accurate predictions and capture the complexity of the underlying data.

Furthermore, the Random Forest classifier also exhibited superior performance in the training data analysis, further validating its efficacy. This classifier utilizes an ensemble approach, building numerous decision trees on subsets of the data and combining their outcomes to enhance prediction accuracy. The strength of this approach lies in its ability to mitigate the limitations of individual decision trees and capture diverse patterns in the data.

However, it is important to acknowledge that the Random Forest classifier has some drawbacks. One notable drawback is its computational requirements and resource-intensive nature, which necessitates substantial computational power to achieve optimal accuracy. Additionally, compared to other models, training the Random Forest classifier may take a longer time due to its ensemble nature and the need to construct multiple decision trees.

Table 2. Internal Validation Performance

Algorithm	Feature Selection	Metric					
		ACC	MCC	ROC	Precision	Recall	Kappa Statistics
BayesNet	No attribute selection	87.43	0.655	0.918	0.878	0.874	0.6544
	CfsSubEval_BestFirst	87.43	0.655	0.918	0.878	0.874	0.654
	CorAttEval_Ranker	87.43	0.655	0.918	0.878	0.874	0.6544
Logistic	No attribute selection	87.43	0.644	0.937	0.873	0.874	0.6439
	CfsSubEval_BestFirst	87.93	0.678	0.939	0.886	0.879	0.6755
	CorAttEval_Ranker	89.94	0.699	0.935	0.893	0.889	0.6982
IBk	No attribute selection	77.88	0.378	0.782	0.779	0.779	0.3779
	CfsSubEval_BestFirst	79.39	0.425	0.872	0.796	0.794	0.4247
	CorAttEval_Ranker	81.40	0.481	0.856	0.816	0.814	0.2088
Random Forest	No attribute selection	90.45	0.720	0.940	0.902	0.905	0.7163
	CfsSubEval_BestFirst	90.45	0.726	0.942	0.903	0.905	0.7251
	CorAttEval_Ranker	90.45	0.726	0.939	0.903	0.905	0.7251

ACC: Accuracy of classification, MCC: Matthews correlation coefficient, ROC: area under the receiver operating characteristic curve

In terms of computational efficiency, our study revealed varying processing times for different models. Specifically, Bayes Net and IBk models completed their training in 0 seconds, while Logistic took 0.01 seconds. On the other hand, the Random Forest classifier required relatively more time, taking approximately 0.04 seconds for training. These time differences can be important considerations when deploying the models in real-world applications that require prompt responses.

3.2. External Validation Performance

In Table 3, we present the performance evaluation of twelve different models on the external validation set, providing insightful statistical results that shed light on the comparative effectiveness of each model. Among these models, the Random Forest classifier with CorAttEval_Ranker feature selection stands out as the top-performing model, demonstrating its exceptional capability in accurately predicting outcomes.

The success rate achieved by the Random Forest model, reaching an impressive 86%, showcases its remarkable predictive power. This high success rate indicates the model's ability to correctly classify instances and accurately predict the unseen data in the external validation set.

Furthermore, the Random Forest model outperforms the other models in several key metrics, highlighting its superiority. Specifically, it exhibits higher values for the MCC (Matthews Correlation Coefficient) at 0.583, Precision at 0.860, and Recall at 0.860 compared to the alternative models. These metrics are essential indicators of the model's performance, demonstrating its ability to strike a balance between true positive and true negative rates, as well as its precision in correctly classifying instances belonging to the positive class.

The exceptional performance of the Random Forest model with CorAttEval Ranker feature selection suggests its suitability for accurately predicting outcomes in this specific context. Its robustness and ability to capture the relevant patterns and relationships in the data set it apart from the other models considered in this study.

Table 3. External Validation Performance

Algorithm	Feature Selection	Metric					
		ACC	MCC	ROC	Precision	Recall	Kappa Statistics
BayesNet	No attribute selection	82.00	0.448	0.865	0.808	0.820	0.4246
	CfsSubEval_BestFirst	82.00	0.448	0.865	0.808	0.820	0.4246
	CorAttEval_Ranker	82.00	0.448	0.865	0.808	0.820	0.4246
Logistic	No attribute selection	84.00	0.539	0.919	0.833	0.840	0.5349
	CfsSubEval_BestFirst	84.00	0.521	0.925	0.831	0.840	0.5050
	CorAttEval_Ranker	84.00	0.521	0.925	0.831	0.840	0.5050
IBk	No attribute selection	78.00	0.380	0.696	0.774	0.780	0.3792
	CfsSubEval_BestFirst	82.00	0.437	0.784	0.817	0.820	0.3836
	CorAttEval_Ranker	76.00	0.304	0.817	0.747	0.760	0.3023
Random Forest	No attribute selection	80.00	0.393	0.893	0.783	0.800	0.3812
	CfsSubEval_BestFirst	84.00	0.513	0.883	0.839	0.840	0.4709
	CorAttEval_Ranker	86.00	0.583	0.893	0.860	0.860	0.5224

ACC: Accuracy of classification, MCC: Matthews correlation coefficient, ROC: area under the receiver operating characteristic curve

By carefully considering these statistical findings, we can confidently assert that the Random Forest model with CorAttEval_Ranker feature selection exhibits the highest performance among the twelve models evaluated for the external validation set. Its impressive success rate and superior values in metrics such as MCC, Precision, and Recall showcase its effectiveness and reinforce its potential as a reliable predictive model for the given problem domain.

Our investigation identified the Troponin T value as the most influential criterion among the thirteen parameters used to build our predictive model. This finding aligns with existing research, which highlights Troponin as a primary biomarker that provides crucial insights into the development of Acute Coronary Syndrome (ACS) [44, 45]. Consequently, our prediction

model's reliance on the Troponin T value reinforces its ability to detect ACS based on this essential biomarker effectively.

By taking into account these factors, including the Random Forest classifier's outstanding performance, its computational requirements, and the significance of the Troponin T value in our predictive model, we can assert that our approach provides a robust and accurate means of diagnosing ACS based on relevant criteria obtained from blood tests.

4. Discussion

The results obtained from the evaluation of the models in Tables 2 and 3 reveal distinct levels of prediction power exhibited by each model. In terms of internal validation, it is evident that the Random Forest (RF) model with CorAttEval_Ranker evaluator stands out as the model with the highest prediction power. The RF model achieved an impressive accuracy rate (ACC) of 90.45%, indicating its suitability and efficacy in predicting early diagnoses of acute coronary syndrome (ACS). This finding emphasizes the RF model's potential in accurately identifying instances of ACS at an early stage, enabling timely intervention and treatment.

Similarly, when considering external validation, the Random Forest model with CorAttEval_Ranker evaluator once again emerges as the frontrunner, boasting a notable percentage rate of 86.00%. This result further supports the notion that the RF model, with its chosen feature selection technique, excels in making accurate predictions on unseen data, reinforcing its reliability and generalizability in real-world scenarios. The findings from our study strongly indicate that the Random Forest algorithm consistently outperforms the other models examined across both internal and external validation. Numerous studies have acknowledged the suitability of Random Forest and similar ensemble models in handling medical data, especially in cardiovascular-related prediction tasks. The robust performance of RF, as demonstrated in our study, reinforces the utility of these models for early ACS diagnosis. However, it is essential to acknowledge the variability in model performance across different datasets and study contexts, as mentioned in our discussion [58,59].

Table 4: The selected parameters

Parameter Selection	Number of Parameters	Parameters
CfsSubsetEval, BestFirst	4	TroponinT CK-MB Age CABG
CorrelationAttributeEval, Ranker	6	Age CK-MB CABG HT TroponinT KAG

CfsSubsetEval: Correlation-based attribute evaluator, CorrelationAttributeEval: Correlation-based attribute evaluator, BestFirst: Search method, Ranker: Search method

Additionally, the emphasis on parameter tuning in our study resonates with the literature's acknowledgment of the critical role that well-calibrated parameters play in enhancing the predictive performance of machine learning models [60, 61]. Table 4 provides an overview of the parameters employed in this study, underscoring their significance in the predictive performance of the Random Forest model with the CorAttEval_Ranker evaluator. By fine-tuning and selecting the appropriate parameters, researchers can enhance the model's ability to capture relevant patterns and accurately predict the desired outcomes.

Cardiac troponins, which were initially described in 1965, emerged as a reliable method for measuring their levels in the blood. However, it was only in the late 1990s that the methodology for assessing cardiac troponins was fully developed. These specific biomarkers indicate cardiac muscle damage and play a crucial role in diagnosing acute coronary syndrome (ACS) [46, 47]. Recent advancements have demonstrated the remarkable sensitivity of troponin detection, even at minimal levels associated with cardiac muscle damage. This heightened sensitivity has contributed to the widespread acceptance of troponin as a standard biomarker for diagnosing ACS, endorsed by esteemed organizations such as the European Society of Cardiology (ESC) and the American College of Cardiology (ACC) since 2000. The specificity and sensitivity of troponin to cardiac muscle damage make it an invaluable tool in diagnosing and monitoring unstable angina pectoris (UAP), a condition recognized by the ACC and the American Heart Association (AHA) [48]. CK-MB is one of the three iso-enzymes of creatine kinase in the heart muscle and 3% of skeletal muscle. It has been reported that, compared to other iso-enzymes, CK-MB is more specific to the myocardium. CK-MB levels rise between 4 and 12 hours after cardiac injury and peak in the blood at 24 hours [49, 50]. Biomarkers associated with troponin, glucose, CK-MB, cholesterol along with age are also used to diagnose COVID-19 with machine learning [13,62,63].

Age is recognized as a significant risk factor for the development of coronary artery disease (CAD). Specifically, individuals who are 45 years or older (for men) and 55 years or older (for women) are considered to be potentially at higher risk for CAD. This association between age and CAD persists even after accounting for other known risk factors. Notably, research has indicated that the probability of developing vascular disease doubles with each passing decade of age, further highlighting the impact of aging on CAD risk [18].

Hypertension, commonly referred to as high blood pressure, represents another silent yet prevalent risk factor for cardiovascular diseases. Numerous studies have demonstrated a strong association between hypertension and cardiovascular conditions, encompassing both elevated systolic and diastolic blood pressure readings. For instance, one study revealed that patients with hypertension exhibited a 63.3% risk of developing coronary artery disease, whereas individuals with normal blood pressure showed a comparatively lower risk of 46.1% [51].

Acute coronary syndrome (ACS) can manifest as a consequence of lesions or blockages occurring in vessels subjected to revascularization through angioplasty, as well as in native or graft vessels used post-surgery, in patients who have previously undergone coronary angiography (CAG) or coronary artery bypass graft surgery (CABG) [52, 53].

Notably, patients with a history of coronary angioplasty or coronary artery bypass graft surgery and subsequently experiencing ACS tend to have a more favorable prognosis compared to individuals with ACS who have not undergone prior interventions. Research findings indicate that the prognosis for patients with prior CAG or CABG who develop ACS is generally more favorable, while those without a history of such interventions tend to have a poorer prognosis [54, 55].

Several limitations should be also considered in the interpretation of our study findings. First, the dataset's representativeness may affect model generalizability, emphasizing the need for diverse datasets. Second, sensitivity to algorithm and feature selection choices underscores considerations for model applicability across datasets. Third, temporal considerations highlight the need for periodic model updates to align with evolving healthcare landscapes. Finally, the clinical applicability of models, including integration into healthcare practices and real-world validation, requires further investigation, presenting avenues for future research.

In summary, our comprehensive analysis highlights the superiority of the Random Forest algorithm, particularly when combined with the CorAttEval Ranker feature selection method, in terms of prediction power for diagnosing ACS. These findings emphasize the importance of selecting appropriate algorithms and parameters to maximize the accuracy and reliability of machine-learning models in specific contexts.

5. Conclusion

In this study, our primary objective was to develop effective machine-learning models for the early diagnosis of acute coronary syndrome (ACS). We constructed twelve distinct machine learning models, leveraging 13 relevant features associated with ACS. Through our analysis, we aimed to identify the most accurate model capable of predicting ACS at its early stages. Our findings demonstrated that the Random Forest algorithm outperformed the other models we developed, showcasing its superior predictive capabilities. This highlights the effectiveness of the Random Forest algorithm in accurately identifying ACS cases early on, potentially enabling timely interventions and treatments.

Furthermore, our analysis revealed that several key parameters play a crucial role in the early diagnosis of ACS. Notably, Troponin T, CK-MB, age, and the presence of coronary artery disease emerged as vital factors for accurate prediction. These findings provide valuable insights into the risk factors and diagnostic indicators associated with acute coronary artery disease. Importantly, the proposed methodology and models developed in this study hold promise for real-world applications beyond ACS diagnosis. By applying similar approaches and feature selection techniques, our models can be adapted to analyze more extensive datasets and explore risk factors for various other diseases. This versatility underscores the potential of our method to contribute to medical research and improve diagnostic practices across different healthcare domains.

In summary, our study contributes to the field of early ACS diagnosis by presenting a robust and accurate machine-learning model. The superior performance of the Random Forest algorithm and the identified key parameters pave the way for improved early detection of ACS. Furthermore, our methodology and models offer potential for broader applications in medical diagnostics, facilitating the identification of risk factors and enhancing our understanding of various diseases when applied to larger datasets.

Ethical Approval

The study was carried out following the principles laid down by the Declaration of Helsinki and received approval from the ethics committee of Karamanoglu Mehmetbey University School of Medicine. Since the research was retrospective in nature, informed consent was not deemed necessary.

Author Contributions

Umut Utku Tiryaki: Conceptualization, Methodology, Software, Validation, Investigation, Data curation, Writing.

Gul Karaduman: Conceptualization, Methodology, Software, Validation, Investigation, Data curation, Writing - Review & Editing, Supervision.

Sare Nur Cuhadar: Conceptualization, Methodology, Investigation.

Ahmet Uyanik: Conceptualization, Methodology, Investigation.

Habibe Durmaz: Conceptualization, Methodology, Investigation, Writing - Review & Editing.

References

- [1] Wilkins, E., Wilson, L., Wickramasinghe, K., Bhatnagar, P., Leal, J., Luengo-Fernandez, R., Burns, R., Rayner, M., Townsend, N., European Cardiovascular Disease Statistics 2017. *European Heart Network*, 2017.
- [2] Thomas, H., Diamond, J., Vieco, A., Chaudhuri, S., Shinnar, E., Cromer, S., Perel, P., Mensah, G. A., Narula, J., Johnson, C. O., Roth, G. A., Moran, A. E., Global Atlas of Cardiovascular Disease 2000-2016: The Path to Prevention and Control. *Global heart*, 13(3), 143–163, 2018.
- [3] World Health Organization, *Cardiovascular Diseases*, 2020.
- [4] Şencan, I., Keskinliç, B., Ekinci, B., Öztemel, A., Sarıoğlu, G., Çobanoğlu, N., Türkiye Kalp ve Damar Hastalıkları Önleme ve Kontrol Programı Eylem Planı (2015-2020). T.C. Türkiye Halk Sağlığı Kurumu. *T.C. Sağlık Bakanlığı Yayın*, 988-1-63,2015.
- [5] Benziger, C. P., Roth, G. A., & Moran, A. E., The Global Burden of Disease Study and the Preventable Burden of NCD. *Global heart*, 11(4), 393–397, 2016.
- [6] Lakic, D., Tasic, L. Kos, M., Economic burden of cardiovascular diseases in Serbia. *Vojnosanit Pregl*, 71(2),137 –143, 2014.
- [7] Maharaj, J.C., Reddy, M., Young Stroke Mortality in Fiji Islands: An Economic Analysis of National Human Capital Resource Loss. *International Scholarly Research Notices*, 802785, 2012.
- [8] Gaziano, T. A., Bitton, A., Anand, S., Weinstein, M. C., & International Society of Hypertension, The global cost of nonoptimal blood pressure. *Journal of hypertension*, 27(7), 1472–1477, 2009.
- [9] Balbay, Y., Gagnon-arpin, I., Malhan, S., Öksüz, M. E., Sutherland, G., Dobrescu, A., Villa, G., Ertuğrul, G., Habib, M., Modeling the burden of cardiovascular disease in Turkey. *Anatol J Cardiol*, 20(4), 235-240, 2018.
- [10] Azambuja, M.I.R., Foppa, M., Maranhao, M.F.C., Achutti, A.C., Economic burden of severe cardiovascular diseases in Brazil: an estimate based on secondary data. *Arq Bras Cardiol*, 91(3),163 –171, 2008.
- [11] Bloom, D., Cafiero, E., McGovern, M., Prettnner, K., Stanciole, A., The Economic Impact of Non-Communicable Disease in China and India: Estimates, Projections, and Comparisons. *The Journal of the Economics of Ageing*, 4,100–111, 2013.
- [12] Dejaco, C., Singh, Y. P., Perel, P., Hutchings, A., Camellino, D., Mackie, S., Abril, A., Bachta, A., Balint, P., Barraclough, K., Bianconi, L., Buttgereit, F., Carsons, S., Ching, D., Cid, M., Cimmino, M., Diamantopoulos, A., Docken, W., Duftner, C., Fashanu, B., et., al. 2015 Recommendations for the management of polymyalgia rheumatica: a European League Against Rheumatism/American College of Rheumatology collaborative initiative. *Arthritis & rheumatology*, 67(10), 2569–2580, 2015.
- [13] Huyut, M. T., Automatic detection of severely and mildly infected COVID-19 patients with supervised machine learning models. *IRBM*, 44(1), 100725, 2023.
- [14] Huyut, M. T., & Huyut, Z., Effect of ferritin, INR, and D-dimer immunological parameters levels as predictors of COVID-19 mortality: A strong prediction with the decision trees. *Heliyon*, 9(3),2023.
- [15] Huyut, M. T., & Üstündağ, H.. Prediction of diagnosis and prognosis of COVID-19 disease by blood gas parameters using decision trees machine learning model: a retrospective observational study. *Medical gas research*, 12(2), 60,2022.
- [16] Kannel, W. B., Coronary heart disease risk factors in the elderly. *The American Journal of geriatric cardiology*, 11(2), 101–107, 2002.
- [17] İkitimur, B., Karadağ, B., Öngen, Z., Yaşlılarda Koroner Arter Hastalığı. *Turkish Journal of Geriatrics*, 2,13-20, 2010.
- [18] Savji, N., Rockman, C. B., Skolnick, A. H., Guo, Y., Adelman, M. A., Riles, T., Berger, J. S., Association between advanced age and vascular disease in different arterial

- territories: a population database of over 3.6 million subjects. *Journal of the American College of Cardiology*, 61(16), 1736–1743, 2013.
- [19] Onat, A., Kaya, A., Şimşek, T., Şimşek, B., Tusun, E., Karadeniz, Y., Can, G., Twenty-five years of the TARF study: The 2015 survey and temporal trends in mortality and loss to follow-up. *Türk Kardiyoloji Dernegi Arsivi*, 44(5),365–370, 2016.
- [20] Yadav, P., Joseph, D., Joshi, P., Sakhi, P., Jha, R. and Gupta, J., Clinical Profile & Risk Factors in Acute Coronary Syndrome. *National Journal of Community Medicine*, 1, 150-151, 2010.
- [21] National Cholesterol Education Program (NCEP) Expert Panel on Detection, Evaluation, and Treatment of High Blood Cholesterol in Adults (Adult Treatment Panel III) . Third Report of the National Cholesterol Education Program (NCEP) Expert Panel on Detection, Evaluation, and Treatment of High Blood Cholesterol in Adults (Adult Treatment Panel III) final report. *Circulation*, 106(25), 3143–3421, 2002.
- [22] Chobanian, A. V., Bakris, G. L., Black, H. R., Cushman, W. C., Green, L. A., Izzo, J. L., Jr, Jones, D. W., Materson, B. J., Oparil, S., Wright, J. T., Jr, Roccella, E. J., Joint National Committee on Prevention, Detection, Evaluation, and Treatment of High Blood Pressure. National Heart, Lung, and Blood Institute, & National High Blood Pressure Education Program Coordinating Committee. Seventh report of the Joint National Committee on Prevention, Detection, Evaluation, and Treatment of High Blood Pressure. *Hypertension*, 42(6), 1206–1252, 2003
- [23] Haffner, S. M., Lehto, S., Rönnemaa, T., Pyörälä, K., & Laakso, M., Mortality from coronary heart disease in subjects with type 2 diabetes and in nondiabetic subjects with and without prior myocardial infarction. *The New England journal of medicine*, 339(4), 229–234,1998.
- [24] Christenson, R. H., Apple, F. S., Morgan, D. L., Alonsozana, G. L., Mascotti, K., Olson, M., McCormack, R. T., Wians, F. H., Jr, Keffer, J. H., & Duh, S. H., Cardiac troponin I measurement with the ACCESS immunoassay system: analytical and clinical performance characteristics. *Clinical chemistry*, 44(1), 52–60, 1998.
- [25] Wu, A. H., Feng, Y. J., Moore, R., Apple, F. S., McPherson, P. H., Buechler, K. F., & Bodor, G., Characterization of cardiac troponin subunit release into serum after acute myocardial infarction and comparison of assays for troponin T and I. American Association for Clinical Chemistry Subcommittee on cTnI Standardization. *Clinical chemistry*, 44, 1198–1208, 1998.
- [26] Bhagavan, N. V., Medical Biochemistry, Chapter 21.3, Energy supply in muscle. *Canada, Acad. Pub*, 122.
- [27] Hillis, G. S., & Fox, K., Cardiac troponins in chest pain can help in risk stratification. *British Medical Journal*, 319(7223), 1451-2, 1999.
- [28] Kocaman, S., Ratlarda deneysel olarak oluşturulacak kalp krizi ve hasarı modeli ile farklı tedavi yöntemlerinin karşılaştırmalı olarak test edilmesi. *PhD Thesis*, 2022.
- [29] Raines, E. W., & Ross, R., Smooth muscle cells and the pathogenesis of the lesions of atherosclerosis. *British heart journal*, 69, S30–S37, 1993.
- [30] Kumbasar, D., Kalp sağlığı, 2013.
- [31] Gaziano T. A., Cardiovascular disease in the developing world and its cost-effective management. *Circulation*, 112(23), 3547–3553, 2005.
- [32] Knuuti, J., Wijns, W., Saraste, A., Capodanno, D., Barbato, E., Funck-Brentano, C., Prescott, E., Storey, R. F., Deaton, C., Cuisset, T., Agewall, S., Dickstein, K., Edvardsen, T., Escaned, J., Gersh, B. J., Svitil, P., Gilard, M., Hasdai, D., Hatala, R., Mahfoud, F., 2019 ESC Guidelines for the diagnosis and management of chronic coronary syndromes: The Task Force for the diagnosis and management of chronic coronary syndromes of the European Society of Cardiology (ESC). *European heart journal*, 41(3), 407–477, 2020.

- [33] Uzun, Ş., Kara, B., İşcan, B. Hemodiyalize giren kronik böbrek yetmezliği olan hastalarda uyku sorunları. *Türk Nefroloji Diyaliz ve Transplantasyon Dergisi*, 12(1): 61-6, 2003.
- [34] Kelleci Çelik, F., Karaduman, G., In silico QSAR modeling to predict the safe use of antibiotics during pregnancy. *Drug and Chemical Toxicology*, 1-10, 2022.
- [35] Frank, Eibe, Mark A. Hall, and Ian H. Witten. *The WEKA workbench*. Morgan Kaufmann, 2016.
- [36] Tang, B., He, H., Baggenstoss, P. M., Kay, S., A Bayesian classification approach using class-specific features for text categorization. *IEEE Transactions on Knowledge and Data Engineering*, 28(6), 1602-1606, 2016 .
- [37] Hogg, R.V., Tanis, E.A., Probability and Statistical Inference. *Upper Saddle River, NJ: Prentice Hall*, 1997.
- [38] Badresiya, A., Vohra, S., Teraiya, J., Performance Analysis of Supervised Techniques for Review Spam Detection. *International Journal of Advanced Networking Applications*, 21–24, 2014.
- [39] Visani, V., Jadeja, N., Modi, M., A Study on Different Machine Learning Techniques for Spam Review Detection. Conference: 2017 International Conference on Energy, Communication, Data Analytics and Soft Computing (ICECDS), 2017.
- [40] Swetha, K., & Ranjana, R., Breast cancer prediction using machine learning and data mining. *International Journal of Scientific Research in Computer Science, Engineering and Information Technology*, 6(3), 610-5, 2020.
- [41] Sridharan, K., & Komarasamy, G., Sentiment classification using random harmony forest and harmony gradient boosting machine. *Soft Computing*, 24(10), 7451-7458, 2020.
- [42] Wang, Z., Chegdani, F., Yalamarti, N., Takabi, B., Tai, B., El Mansori, M., & Bukkapatnam, S., Acoustic Emission Characterization of Natural Fiber Reinforced Plastic Composite Machining Using a Random Forest Machine Learning Model. *Journal of Manufacturing Science and Engineering*, 142(3), 031003, 2020.
- [43] Viera, A. J., Garrett, J. M., Understanding interobserver agreement: the kappa statistic. *Family medicine*, 37(5), 360-363, 2005.
- [44] Gerhardt, W., Katus, H. A., Ravkilde, J., Hamm, C., Jørgensen, P. J., Peheim, E., Ljungdahl, L., Löfdahl, P., S-troponin T in suspected ischemic myocardial injury compared with mass and catalytic concentrations of S-creatine kinase isoenzyme MB. *Clinical chemistry*, 37(8), 1405–1411, 1991.
- [45] Hamm, C.W., Goldmann, B.U., Heeschen, C., Kreymann, G., Berger, J., Meinertz, T., Emergency room triage of patients with acute chest pain by means of rapid testing for cardiac troponin T or troponin. *New England Journal of Medicine*, 337 (23), 1648-1653, 1997.
- [46] Ebashi, S., Kodama, A., A new protein factor promoting aggregation of tropomyosin. *Journal of biochemistry*, 58(1), 107–108, 1965.
- [47] Tahir, K., Pauley, E., Dai, X., Smith, S. C., Jr, Sweeney, C., & Stouffer, G. A., Mechanisms of ST Elevation Myocardial Infarction in Patients Hospitalized for Noncardiac Conditions. *The American journal of cardiology*, 123(9), 1393–1398, 2019.
- [48] Sheehan, P., Vasikaran, S.D. The evolving clinical role of cardiac troponins and new acute myocardial infarction guidelines: Implications for the clinical laboratory. *Clin Bichemist Rev*, 23,52-65,2001.
- [49] Reichlin, T., Hochholzer, W., Bassetti, S., Steuer, S., Stelzig, C., Hartwiger, S., Biedert, S., Schaub, N., Buerge, C., Potocki, M., Noveanu, M., Breidhardt, T., Twerenbold, R., Winkler, K., Bingisser, R., Mueller, C., Early diagnosis of myocardial infarction with sensitive cardiac troponin assays. *The New England journal of medicine*, 361(9), 858–867, 2009.

- [50] Hornemann, T., Dorothea, R., Wallimann, T., Why is creatine kinase a dimer? Evidence for cooperativity between the two subunits. *Biochimica et Biophysica Acta (BBA)-Protein Structure and Molecular Enzymology*, 1480.1,365-373, 2000.
- [51] Hebert, P. R., Moser, M., Mayer, J., Glynn, R. J., & Hennekens, C. H., Recent evidence on drug therapy of mild to moderate hypertension and decreased risk of coronary heart disease. *Archives of internal medicine*, 153(5), 578–581,1996.
- [52] Campeau, L., Lesperance, J., Bourassa, M.G., Natural history of saphenous vein aortocoronary bypass grafts. *Mod Concepts Cardiovasc Dis* 1984,53:59-63.
- [53] Fitzgibbon, G. M., Kafka, H. P., Leach, A. J., Keon, W. J., Hooper, G. D., & Burton, J. R., Coronary bypass graft fate and patient outcome: angiographic follow-up of 5,065 grafts related to survival and reoperation in 1,388 patients during 25 years. *Journal of the American College of Cardiology*, 28(3), 616–626, 1996.
- [54] Labinaz, M., Mathias, J., Pieper, K., Granger, C. B., Lincoff, A. M., Moliterno, D. J., Van de Werf, F., Simes, J., White, H. D., Simoons, M. L., Califf, R. M., Topol, E. J., Armstrong, P. W., Harrington, R. A., Outcomes of patients with acute coronary syndromes and prior percutaneous coronary intervention: a pooled analysis of three randomized clinical trials. *European heart journal*, 26(2), 128–136, 2005.
- [55] Lee, K. L., Woodlief, L. H., Topol, E. J., Weaver, W. D., Betriu, A., Col, J., Simoons, M., Aylward, P., Van de Werf, F., Califf, R. M., Predictors of 30-day mortality in the era of reperfusion for acute myocardial infarction. Results from an international trial of 41,021 patients. *Circulation*, 91(6), 1659–1668, 1995.
- [56] Karaduman, G., Kelleci Çelik, F., 2D-Quantitative structure-activity relationship modeling for risk assessment of pharmacotherapy applied during pregnancy. *Journal of Applied Toxicology*, 43(10), 1436-1446, 2023.
- [57] Erturan, A. M., Karaduman, G., Durmaz, H., Machine learning-based approach for efficient prediction of toxicity of chemical gases using feature selection. *Journal of Hazardous Materials*, 455, 131616, 2023.
- [58] Raihan, M., Islam, M. M., Ghosh, P., Shaj, S. A., Chowdhury, M. R., Mondal, S., & More, A., A comprehensive Analysis on risk prediction of acute coronary syndrome using machine learning approaches. In 2018 21st International Conference of Computer and Information Technology (ICIT) (pp. 1-6). IEEE, 2018.
- [59] Ke, J., Chen, Y., Wang, X., Wu, Z., Zhang, Q., Lian, Y., & Chen, F., Machine learning-based in-hospital mortality prediction models for patients with acute coronary syndrome. *The American journal of emergency medicine*, 53, 127-134, 2022.
- [60] Huang, Z., Ge, Z., Dong, W., He, K., Duan, H., & Bath, P., Relational regularized risk prediction of acute coronary syndrome using electronic health records. *Information Sciences*, 465, 118-129, 2018.
- [61] Bouzid, Z., Faramand, Z., Gregg, R. E., Frisch, S. O., Martin-Gill, C., Saba, S., ... & Al-Zaiti, S., In search of an optimal subset of ECG features to augment the diagnosis of acute coronary syndrome at the emergency department. *Journal of the American Heart Association*, 10(3), e017871, 2021.
- [62] Huyut, M. T., & Ilkbahar, F., The effectiveness of blood routine parameters and some biomarkers as a potential diagnostic tool in the diagnosis and prognosis of Covid-19 disease. *International Immunopharmacology*, 98, 107838, 2021.
- [63] Huyut, M. T., Huyut, Z., Ilkbahar, F., & Mertoğlu, C., What is the impact and efficacy of routine immunological, biochemical and hematological biomarkers as predictors of COVID-19 mortality?. *International Immunopharmacology*, 105, 108542, 2022.



Effect of Temperature on Damage Identification of Laminated Composite by Means Numerical Methods

Mehmet Ali Akin ^{a*}, Bülent Ekici ^b

^{a,b} Marmara University Institute of Pure and Applied Sciences, Istanbul, Turkey

✉: maliakin3@gmail.com ^{a*}, bulent.ekici@marmara.edu.tr ^b,  ID: 0009-0002-4185-8209 ^{a*}, 0000-0001-8967-0649 ^b

Received: 20.12.2023, Revised: 01.03.2024, Accepted: 01.03.2024

Abstract

This study aims to examine the effect of temperature on damage detection in laminated composite materials. In this context, a carbon-reinforced composite plate with [0/90]_s stacking sequence is modeled as intact and delaminated by the finite element method. The dimensions, thicknesses, materials used, and stacking sequences of the plates modeled as intact and delaminated are the same. The delamination in the delaminated plate is modeled as the gap in the middle of the plate. These modeled plates were analyzed at different temperature values between -50oC / +50oC. The natural frequencies, mode shapes, and modal curvatures of the plate were obtained by modal analysis. The variation of these data obtained with temperature was examined and the effect of temperature on these data was compared. According to the analysis results, it was observed that the effect of temperature on natural frequency values and modal curvature values was similar to the effect of delamination. The decrease in natural frequencies and the changes in modal curvatures due to delamination occurred with the increase in temperature even in the absence of delamination.

Keywords: Composites, Damage Identification, Numerical Methods, Temperature Effect.

1. Introduction

Damage detection in composite materials is crucial to maintaining structural integrity and safety. Modal analysis techniques are useful for identifying damage. The variations in modal curvatures are taken into account in this context as a signal for locating probable damage locations in composite materials [1, 2, 3, 4]. Natural frequencies and mode shapes of a material structure are used to identify the property known as modal curvature. Due to the presence or extent of damage, the modal curvatures of a damaged composite structure may alter [5]. Between modal curvatures, there is a noticeable variation in plate structure due to intrinsic degradation, particularly delamination [6]. For damage detection, modal curvatures in a predetermined intact reference state are compared with modal curvatures in a damaged structure [6]. The modal curvature difference serves as an indicator used to determine the location and extent of damage [7].

Composite materials are materials that are formed by combining different components and generally have superior mechanical properties. However, the different temperature environments to which composite structures are exposed can significantly affect material performance [8]. Temperature can also affect the mechanical properties of composite materials. Composite materials may show different mechanical properties at different temperature values [9,10]. While an increase in temperature causes a decrease in the stiffness and strength of the material, a decrease in temperature may cause the opposite effect [11].

Stiffness changes are very important in terms of vibration-based detection methods, which is one of the damage detection methods [12]. Vibration-based damage detection methods evaluate hardness changes to identify damaged areas using frequency changes in material or structure or



changes in modal parameters. Therefore, changes in the mechanical structure of the material under the influence of temperature may affect damage detection.

However, the effect of temperature on damage detection in laminated composites is a complex and under-researched issue. In this context, this study aims to fill a critical gap in the existing literature by investigating the effect of temperature on the structural properties of laminated composite materials. The main contributions of this study include a comprehensive examination of the natural frequencies, mode shapes, and modal curvatures of composite materials. The most fundamental innovation provided by this study is to integrate the temperature effect into damage detection analysis and pave the way for the creation of more durable and reliable composite structures in dynamic environmental conditions. This study not only provides an understanding of the interaction between temperature and damage detection but also provides practical information that can be applied in various industries. Understanding the effect of temperature on the behavior of laminated composites also provides advantages in preserving the structural integrity, health monitoring, and extending the lifespan of composite materials used in fields such as aerospace, automotive, wind energy, and construction.

2. Analytical Theory

Any composite construction has internal stresses known as thermal residual stresses that develop during the composite's curing process. Composite plates that cure at temperatures other than the specified operating temperature experience thermal stresses and these stresses must be considered in the analysis. These stresses are inherent to the structure. The discrepancy between the matrix's and fiber's coefficients of thermal expansion is what causes them to form. Thermal residual stresses brought on by this shrinkage must be considered in any stress analysis of the composite structure and should not be disregarded. Residual stress limits the strength potential of composite materials.

According to classical laminate theory, thermal moments and resultant moments in composite materials are defined as follows, respectively.

$$\begin{bmatrix} M_x^T \\ M_y^T \\ M_{xy}^T \end{bmatrix} = \int \begin{bmatrix} \bar{Q}_{11} & \bar{Q}_{12} & \bar{Q}_{16} \\ \bar{Q}_{12} & \bar{Q}_{22} & \bar{Q}_{26} \\ \bar{Q}_{16} & \bar{Q}_{26} & \bar{Q}_{66} \end{bmatrix}_k \begin{bmatrix} \alpha_x \\ \alpha_y \\ \alpha_{xy} \end{bmatrix}_k \Delta T z dz \quad (1)$$

$$\begin{bmatrix} M_x \\ M_y \\ M_{xy} \end{bmatrix} = \begin{bmatrix} B_{11} & B_{12} & B_{16} \\ B_{12} & B_{22} & B_{26} \\ B_{16} & B_{26} & B_{66} \end{bmatrix} \begin{bmatrix} \varepsilon_x^0 \\ \varepsilon_y^0 \\ \gamma_{xy}^0 \end{bmatrix} + \begin{bmatrix} D_{11} & D_{12} & D_{16} \\ D_{12} & D_{22} & D_{26} \\ D_{16} & D_{26} & D_{66} \end{bmatrix} \begin{bmatrix} k_x^0 \\ k_y^0 \\ k_{xy}^0 \end{bmatrix} - \begin{bmatrix} M_x^T \\ M_y^T \\ M_{xy}^T \end{bmatrix} \quad (2)$$

Where M^T represents thermal moments, M represents resultant moments, \bar{Q}_{ij} is the transformed reduced stiffnesses, α is the thermal coefficient, k is the layer number and ΔT is the temperature change, z is the directed distance, B_{ij} is bending-extension coupling stiffnesses and D_{ij} is bending stiffnesses, ε^0 is middle surface shear stress and k^0 is the middle-surface curvatures.

Equation (2) can be rearranged and written as:

$$\begin{bmatrix} \bar{M}_x \\ \bar{M}_y \\ \bar{M}_{xy} \end{bmatrix} = \begin{bmatrix} M_x + M_x^T \\ M_y + M_y^T \\ M_{xy} + M_{xy}^T \end{bmatrix} = \begin{bmatrix} B_{11} & B_{12} & B_{16} \\ B_{12} & B_{22} & B_{26} \\ B_{16} & B_{26} & B_{66} \end{bmatrix} \begin{bmatrix} \varepsilon_x^0 \\ \varepsilon_y^0 \\ \gamma_{xy}^0 \end{bmatrix} + \begin{bmatrix} D_{11} & D_{12} & D_{16} \\ D_{12} & D_{22} & D_{26} \\ D_{16} & D_{26} & D_{66} \end{bmatrix} \begin{bmatrix} k_x^0 \\ k_y^0 \\ k_{xy}^0 \end{bmatrix} \quad (3)$$

If the equation is rearranged to isolate curvatures on one side;

$$\begin{bmatrix} k_x^0 \\ k_y^0 \\ k_{xy}^0 \end{bmatrix} = \begin{bmatrix} D_{11} & D_{12} & D_{16} \\ D_{12} & D_{22} & D_{26} \\ D_{16} & D_{26} & D_{66} \end{bmatrix}^{-1} \begin{bmatrix} \bar{M}_x \\ \bar{M}_y \\ \bar{M}_{xy} \end{bmatrix} - \begin{bmatrix} D_{11} & D_{12} & D_{16} \\ D_{12} & D_{22} & D_{26} \\ D_{16} & D_{26} & D_{66} \end{bmatrix}^{-1} \begin{bmatrix} B_{11} & B_{12} & B_{16} \\ B_{12} & B_{22} & B_{26} \\ B_{16} & B_{26} & B_{66} \end{bmatrix} \begin{bmatrix} \varepsilon_x^0 \\ \varepsilon_y^0 \\ \gamma_{xy}^0 \end{bmatrix} \quad (4)$$

Modal curvature is calculated as second-order differentiation of mode shape. [1]

$$k = k_x + k_y = \frac{\partial^2 w(x, y)}{\partial x^2} + \frac{\partial^2 w(x, y)}{\partial y^2} \quad (5)$$

Where k_x and k_y are the modal curvatures along the X and Y-axis.

To find the damage factor, modal curvature differences of the delaminated composite plate and the reference composite plate are calculated. In regions where delamination occurs, modal curvatures increase due to a decrease in the stiffness of the composite lamina. Mode shapes obtained as a result of Finite Element Analysis (FEA) can be used to determine modal curvatures by central difference approximation. [1] Mathematically, X and Y axis-directed modal curvatures are [6];

$$k_x = \frac{w_{(i-1),j} - 2w_{i,j} + w_{(i+1),j}}{h^2} \quad (6)$$

$$k_y = \frac{w_{i,(j-1)} - 2w_{i,j} + w_{i,(j+1)}}{h^2} \quad (7)$$

Where w_{ij} is mode shape at i^{th} row and j^{th} column and h is the total thickness.

Absolute change in modal curvature is calculated as [6];

$$k = k_x + k_y = [D]^{-1} \left([\bar{M}_x + \bar{M}_y] - [B] [\varepsilon_x^0 + \varepsilon_y^0] \right) \quad (9)$$

It is known that the damage to the composite laminate causes alterations in the mechanical characteristics of the composite lamina. For this reason, in case of damage to the composite

lamina, changes in the mechanical properties of the lamina will also cause changes in the modal curvature. However, changes in the temperature of the laminate will also cause changes in the thermal loads, as seen in the equation (9). Due to changing thermal loads, the modal curvature will change and differ from the reference value.

3. Finite Element Modal Curvature Analysis

In this study, to understand the dynamic structures of laminated composites under changing temperature conditions, thermal stresses were first applied to the plates, and then the plates were subjected to modal analysis. This method is called pre-stress analysis. ANSYS pre-stress analysis has been a good tool for extracting natural frequencies, mode shapes, and modal curvatures. The novelty of this approach lies in the careful application of thermal stresses and the relationship between the layers of the plate during pre-stress analysis. Thus, it is aimed to make a reliable simulation of the behavior of laminated composites under real conditions. The real conditions that composite structures are exposed to in practice are reflected by including thermal residual stresses and thermal moments in the analysis. With this application, the accuracy of the results has been increased.

Modal analysis was performed using a four-layered composite plate which has a 100 x 100 mm surface area and 1 mm thickness with a [0/90]_s stacking sequence. Plates with temperature values of -50°C, -40°C, -30°C, -22°C, 0°C, 22°C, 30°C, 40°C, 50°C were analyzed in the analysis. In addition, a composite plate having the same dimensions with a delamination area of 20 mm x 20 mm with the same temperature values was evaluated. All of the composite plates are fixed at their edges, having the same fixed boundary conditions.

Unidirectional carbon fiber material was used and the material properties were defined as follows.

Table 1. Natural Frequencies of the Delaminated Composite Plate

Mechanical Properties	
Density	1518 Kg/m ³
Young's Modulus X Direction	1,2334E+11 Pa
Young's Modulus Y Direction	7,78E+09 Pa
Young's Modulus Z Direction	7,78E+09 Pa
Poisson's Ratio XY	0,27
Poisson's Ratio YZ	0,42
Poisson's Ratio XZ	0,27
Shear Modulus XY	5E+09 Pa
Shear Modulus YZ	3,08E+09 Pa
Shear Modulus XZ	5E+09 Pa

Geometrically, the material is defined as a 2D square plate with dimensions of 100 mm x 100 mm, and this modeling process was also done using ANSYS.

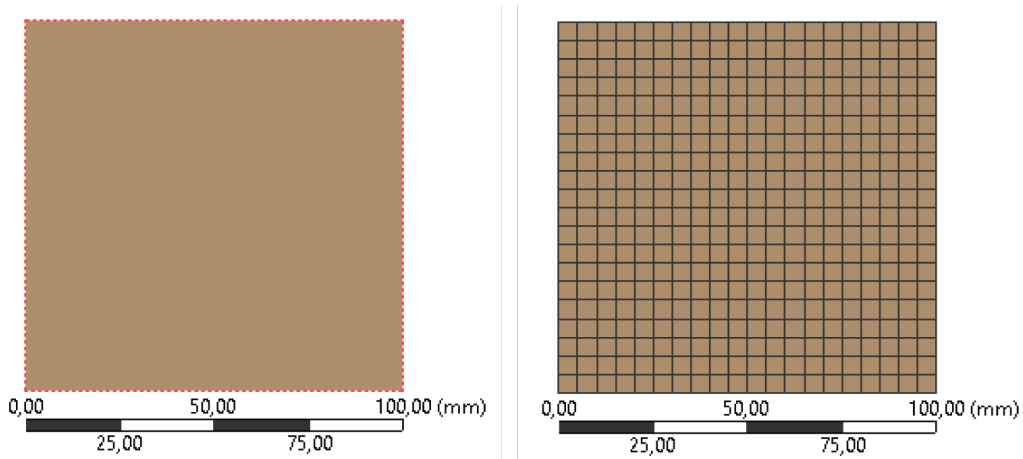


Fig. 1. Geometry and Mesh Model of Intact Composite Material

By using the same geometry, empty space was defined in the structure and the delamination was modeled as in Figure 2.

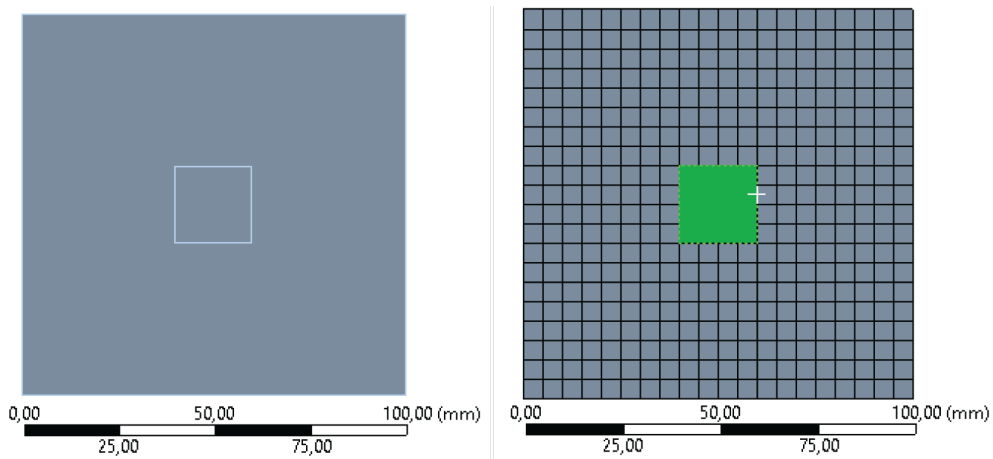


Fig. 2. Geometry and Mesh Model of Delaminated Composite Material

The natural frequencies of these structures were discovered by the modal analysis, and they are shown in Tables 2 and 3.

Table 2. Natural Frequencies of the Intact Composite Plate

Temperature / Natural Frequencies									
Mode Number	-50°C	-40°C	-30°C	-22°C	0°C	22°C	30°C	40°C	50°C
1	542,97	532,68	522,07	513,35	488,12	470,81	450,28	436,6	422,29
2	878,14	865,12	851,57	840,33	807,37	770,98	756,78	738,2	718,62
3	1873	1863,7	1854,2	1846,5	1825	1802,9	1794,6	1784,2	1773,5
4	1949,6	1938,2	1926,4	1916,8	1889,3	1859,9	1848,7	1834,1	1819

Table 3. Natural Frequencies of the Delaminated Composite Plate

Mode Number	Temperature / Natural Frequencies								
	-50°C	-40°C	-30°C	-22°C	0°C	22°C	30°C	40°C	50°C
1	522,8	514,84	506,69	500,03	480,97	470,72	453,02	443,11	432,87
2	802,77	792,33	781,53	772,61	746,74	719	704,78	690,63	675,84
3	1751,2	1743,8	1736,3	1730,4	1713,8	1698,4	1689,2	1681,6	1129,3
4	1915,6	1908	1900,2	1893,7	1874,6	1853,4	1844,7	1833,1	1820,4

As can be seen from Tables 2 and 3, the natural frequencies of the intact plate decrease as the temperature increases, the same is true for the delaminated plate. When looking at the natural frequencies for intact and delaminated plates at the same temperatures, it is seen that the natural frequency of the delaminated plate is lower than that of the intact plate. This is a result consistent with previous studies.

3.1. Mode shape deformations

The first mode’s natural frequency and the mode shape of the plates were assessed. Analysis results were extracted and the obtained mode shape deformations were compared. Mode shape deformations occurring at -50oC, 0oC, and 50oC are given in Figure 3, Figure 4, and Figure 5.

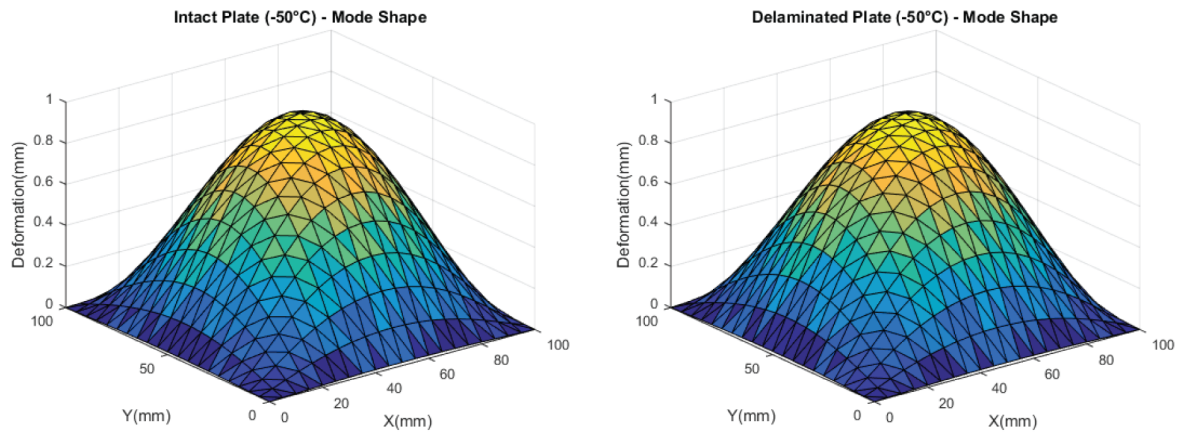


Fig. 3. Intact and Delaminated Plates Mode Shapes at -50°C

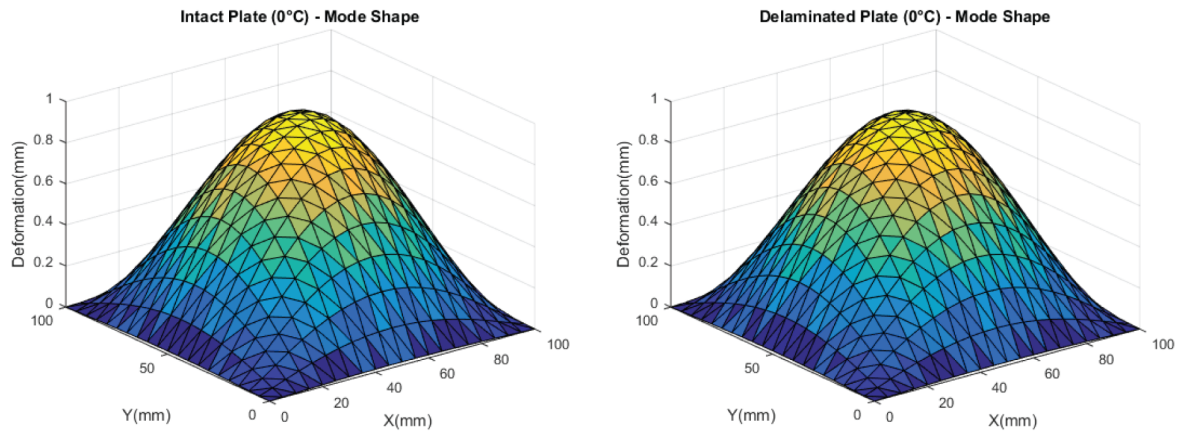


Fig. 4. Intact and Delaminated Plates Mode Shapes at 0°C

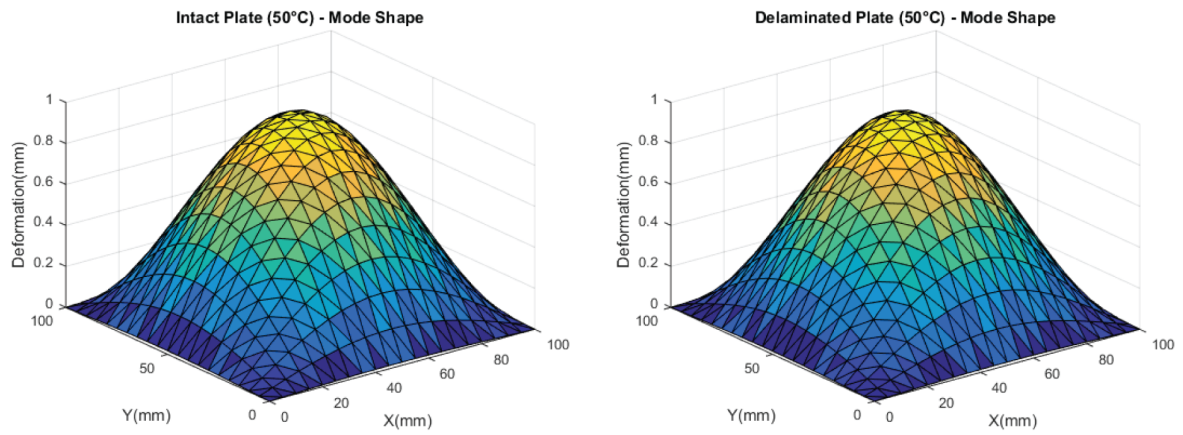


Fig. 5. Intact and Delaminated Plates Mode Shapes at 50°C

It is shown in the figures above that the results of the mode shapes are quite similar and there is no clear distinguishing difference between intact and delaminated plates. For this reason, it is very difficult to comment on the temperature effect on the detection of the damage or whether there is any damage according to the mode shapes in the plate.

3.2. Normalized modal curvatures

The modal curvatures for intact and delaminated plates were calculated at different temperatures using the equations (5), (6), (7) and (8). Modal curvature changes occurring at -50°C, 0°C, and 50°C are given in Figure 6, Figure 7, and Figure 8.

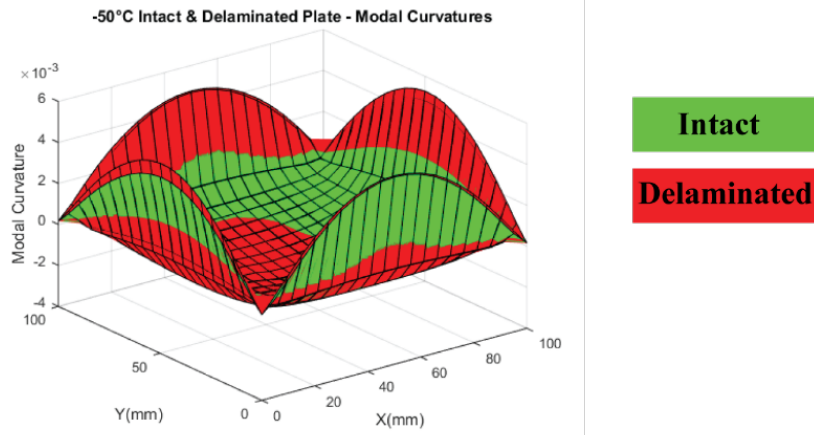


Fig. 6. Intact and Delaminated Plates Modal Curvatures at -50°C

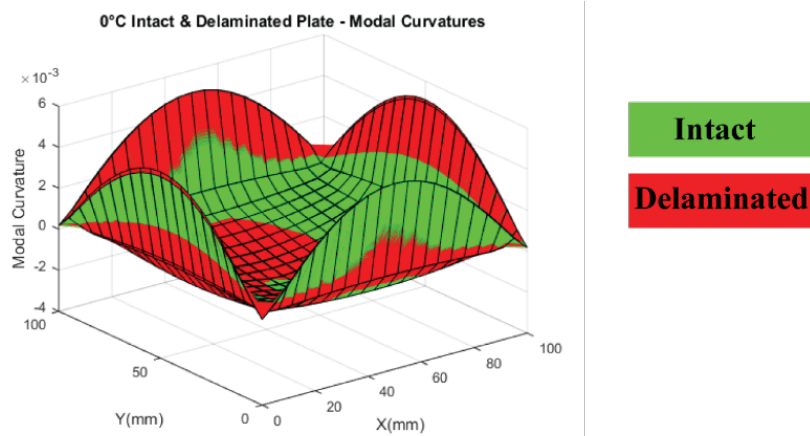


Fig. 7. Intact and Delaminated Plates Modal Curvatures at 0°C

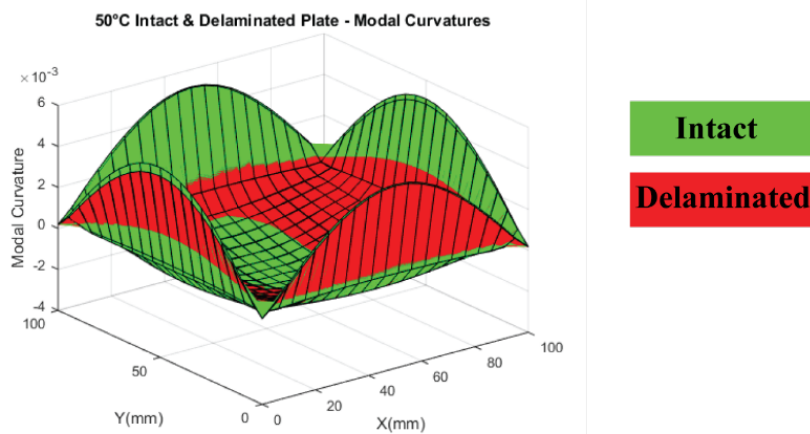


Fig. 8. Intact and Delaminated Plates Modal Curvatures at 50°C

The modal curvature change by the effect of the temperature and delamination at the middle of the plates and the left edge of the plates are shown in Figure 10 and Figure 11.

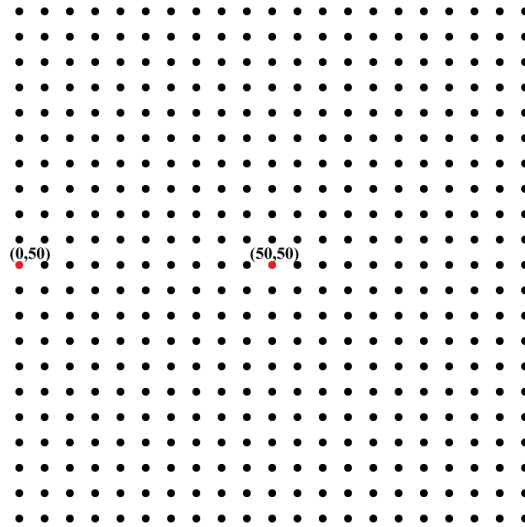


Fig. 9. Nodes On The Plate

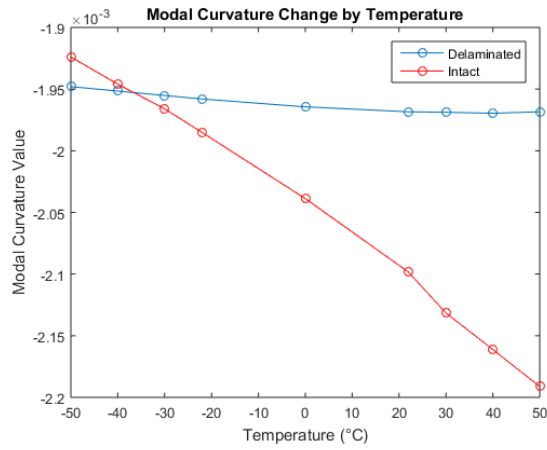


Fig. 10. Modal Curvature Differences at Node (50,50)

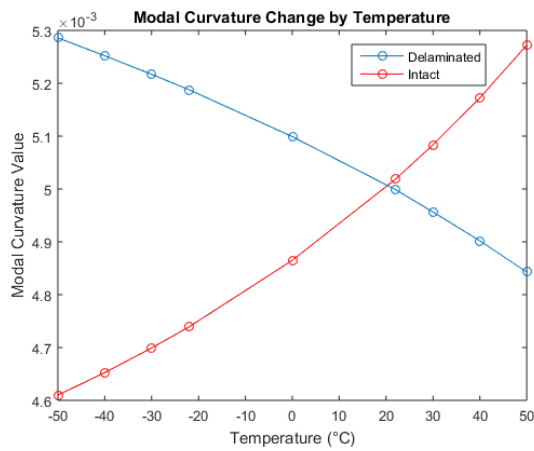


Fig. 11. Modal Curvature Differences at Node (0,50)

The graphs show that the temperature change causes a change in the modal curvatures of the intact plate. Additionally, at the same temperatures, variations are seen between the intact and delaminated plate modal curvatures.

4. Conclusion

In this study, ANSYS Pre-stress analysis was employed to assess the modal curvatures, mode shapes, and natural frequencies of intact and delaminated plates at various temperature levels. The acquired results support previous research and demonstrate that the natural frequencies of the plates decrease as temperature rises [13, 14, 15]. Additionally, it was found that the delaminated plates' natural frequencies were significantly impacted by the temperature increase. Loss of stiffness and a drop in frequency are results of delamination. Delamination results in a truncated region in the plate structure, which reduces frequency and causes a loss of stiffness. [16] The temperature states of the plates play a significant influence on the natural frequencies and dynamic behavior of plates, which are better understood as a result of these findings.

Based on these findings, it has been observed that the decrease in natural frequencies and the change in modal curvatures with the increase in temperature in composite materials are very similar to the results of delamination occurring in the composite material. Therefore, observing these changes in material properties and making an inference that there is delamination in the material is insufficient to reach a definitive conclusion. This demonstrates the need to understand the effect of temperature on composite materials and include it in health monitoring analyses. In this way, by eliminating the temperature effect, the material can be monitored more accurately and a more accurate result can be reached as to whether there is delamination on the material.

In summary, with this study, the effect of temperature on the dynamic behavior of the plates and the importance of considering temperature factors in structural integrity assessment and damage detection are emphasized. Additionally, temperature-dependent effects on damage detection have been brought to light by comparing modal curvatures between intact and delaminated plates. These findings contribute significantly to the understanding of composite material behavior under various environmental conditions. Advanced simulation tools such as the ANSYS Pre-Stress Analysis methodology are used to pave the way for future developments in the application of composite materials. The vital role of temperature considerations in structural analysis is recognized, deepening this understanding of laminated composites and paving the way for more accurate and reliable evaluations in practical applications. In addition, the proposed solution methodology stands out with its ability to distinguish temperature-dependent effects in damage detection, an aspect often overlooked in traditional studies.

Author Contributions

Mehmet Ali Akin: Collected the data, Contributed data or analysis tools, Wrote the paper.
Bülent Ekici: Conceived and designed the analysis.

References

- [1] Pandey, A. K., Biswas, M. and Samman, M. M., Damage detection from changes in curvature mode shapes, *Journal Of Sound And Vibration*, 321-332, 1991.

- [2] Hasrizam, C.M., Fawazi, N., Damage identification based on curvature mode shape using cubic polynomial regression and chebyshev filters, *IOP Conf. Ser.: Mater. Sci. Eng.*, 271 012091, 01 Nov 2017.
- [3] Chandrashekhar, M. and Ganguli, R., Structural damage detection using modal curvature and fuzzy logic, *Structural Health Monitoring*, 8, 267, 2009.
- [4] Dawari, V. B., Vesmawala, G. R., Structural damage identification using modal curvature differences, *Journal of Mechanical and Civil Engineering*, 33-38, 2013.
- [5] Lestari, W., Qlao P., Hangud, S., Curvature mode shape-based damage assessment of carbon/epoxy composite beams, *Journal of Intelligent Material Systems and Structures*, 18(3),189-208, 2007.
- [6] Naidu, S., Ratnam, C., Rambabu, G., Delamination identification of composites using normalized modal curvature and image processing, *International Journal Of Engineering Research & Technology (IJERT)*, 9(09), 2020.
- [7] Hamey, C. S., Lestari, W., Qiao, P., and Song, G., Experimental damage identification of carbon/epoxy composite beams using curvature mode shapes, *Structural Health Monitoring*, 3(4), 0333–353, 2004.
- [8] Salim, B., Chabira, S. F., Bolland, P., Mohamed, S., Soufiane, B., Thermal aging effect on the mechanical properties of polyester fiberglass composites, *J. Mater. Environ. Sci.*, 6 (10), 2795-2803, 2015.
- [9] Colakoglu, M., Effect of temperature on frequency and damping properties of polymer matrix composites, *Advanced Composite Materials*, 17(2), 111-12, 2008.
- [10] Jia, Z., Li, T., Chiang, F., and Wang, L., An experimental investigation of the temperature effect on the mechanics of carbon fiber reinforced polymer composites, *Composites Science and Technology*, 154, 2017.
- [11] Liu, J., Zhou, Z., Ma, L., Xiong, J., Wu, L., Temperature effects on the strength and crushing behavior of carbon fiber composite truss sandwich cores, *Composites Part B: Engineering*, Volume 42, Issue 7, 1860-1866, 2011.
- [12] Lakhdera, M., Mohammeda, D., Boudjemâaa, L., Rabiâa, A., Bachira, M., Damages detection in a composite structure by vibration analysis, *TerraGreen 13 International Conference*, Beirut, Lebanon, 15-17 Feb. 2013.
- [13] Liu, H. Wang, X. Jiao, Y., Effect of temperature variation on modal frequency of reinforced concrete slab and beam in cold regions. *Shock and Vibration*, 1–17, 2016.
- [14] Kim, J.-T., Park, J.-H., Lee, B.-J., Vibration-based damage monitoring in model plate-girder bridges under uncertain temperature conditions, *Engineering Structures*, 29, 1354–1365., 2007
- [15] Zhou, Y. Sun, L., Effects of environmental and operational actions on the modal frequency variations of a sea-crossing bridge: A periodicity perspective, *Mech. Syst. Signal Process*, 131, 505–523, 2019.
- [16] Khan, A., Kim, H.S., A brief overview of delamination localization in laminated composites, *Multiscale Sci. Eng.* 4, 102–110, 2022.




Investigation of Pedestrian and Driver Behaviors at Push-Button Crosswalk on Main Arterials of Urban Roads: A Case of Samsun City, Türkiye

Eren Dağlı^{a*}, Ahmet Göktuğ Saraç^b, Metin Mutlu Aydın^c

^aSelcuk University, Doganhisar Vocational School, Konya, Turkey

^{b,c}Ondokuz Mayıs University, Faculty of Engineering, Department of Civil Engineering, Samsun, Turkey

✉ : eren.dagli@selcuk.edu.tr^{a*}, ahmetgsarac@hotmail.com^b, metinmutluaydin@gmail.com^c

 : 0000-0002-3892-0270^{a*}, 0009-0007-8969-0384^b, 0000-0001-9470-716X^c

Received: 23.01.2024, Revised: 03.03.2024, Accepted: 13.03.2024

Abstract

There are different types of crosswalks for pedestrians to cross the street and different methods of operation. Signalization can be used in the operation of at-grade and controlled crosswalk. In these crosswalks, signaling is activated by pedestrians pressing buttons placed on the crosswalks. In this type of crossing, pedestrians press the button to cross the road and the signaling system detects the request. Within a reasonable time, the system turns red for vehicles and green for pedestrians, allowing pedestrians to cross the street safely. However, these systems have some drawbacks. Various observation and data collection studies were carried out at the pilot pedestrian crossing on Atatürk Boulevard in Atakum district of Samsun province. In these studies, 227 pedestrians crossing the crosswalk and 791 vehicles stopped at red lights during the crossing of pedestrians were examined. As a result of the data obtained in line with pedestrian and driver behaviors, it is aimed to determine the operational problems in signalized crosswalk with pedestrian warning and to increase efficiency with the studies to be carried out.

Keywords: Crosswalk, push-button crosswalk, traffic accidents, pedestrian safety, traffic lights

1. Introduction

Unpredictable accidents that can occur at any time as a result of negligence and erroneous behavior can result in loss of life and property [1]. Traffic accidents are unpredictable events that occur on the highway, in which vehicles, drivers and pedestrians are involved separately or together, and which cause various negative effects as a result. [2].

Population growth and the parallel increase in the number of motorized vehicles increase traffic accidents [3]. Table 1 shows the number of vehicles registered to traffic, the total number of accidents and the number of deaths, injuries and material losses as a result of accidents between 2013 and 2022 [4]. As can be seen from the table, the number of vehicles registered to traffic increases regularly every year. The number of traffic accidents is expected to decrease with the developing vehicle technologies and intelligent transportation systems applications. However, when we look at the number of accidents, high numbers of accidents are noteworthy throughout all years. Only in 2020, there is a significant decrease in the total number of accidents. This situation is thought to be caused by the curfews imposed as a result of the Covid-19 pandemic. It is a fact that the pandemic process has caused large and irregular changes in traffic flow and the number of vehicles [5]. Although the number of deaths and injuries as a result of traffic accidents increased significantly between 2015-2017, it has been in a downward trend after 2017.



Table 1. Number of vehicles registered, accidents, persons killed and injured, 2013-2022 [4]

Year	Number of vehicles registered to traffic	Total number of accidents	Number of accidents involving death or injury	Number of accidents involving material loss only	Number of person killed	Number of person injured
2013	17.939.447	1.207.354	161.306	1.046.048	3.685	274.829
2014	18.828.721	1.199.010	168.512	1.030.498	3.524	285.059
2015	19.994.472	1.313.359	183.011	1.130.348	7.530	304.421
2016	21.090.424	1.182.491	185.128	997.363	7.300	303.812
2017	22.218.945	1.202.716	182.669	1.020.047	7.427	300.383
2018	22.865.921	1.229.364	186.532	1.042.832	6.675	307.071
2019	23.156.975	1.168.144	174.896	993.248	5.473	283.234
2020	24.144.857	983.808	150.275	833.533	4.866	226.266
2021	25.249.119	1.186.353	187.963	998.390	5.362	274.615
2022	26.482.847	1.232.957	197.261	1.035.696	5.229	288.696
Total	221.971.728	11.905.556	1.777.553	10.128.003	53.547	2.848.386

Table 2 shows the distribution of victims in fatal and injury traffic accidents in 2022 in terms of drivers, passengers and pedestrians. Pedestrians account for 23.2% of fatalities and 12.8% of injuries in traffic accidents [4]. Pedestrian-oriented studies are also needed to eliminate the negative consequences of traffic accidents. The vulnerability of pedestrians to collisions makes the consequences of accidents more serious [6]. The risk of death and injury increases in accidents caused by vehicles hitting pedestrians.

Table 2. Number of victims of traffic accidents involving death or injury, 2022 [4]

Victims		
Driver	Number of persons killed	2.349
	Number of persons injured	141.795
Passenger	Number of persons killed	1.662
	Number of persons injured	109.790
Pedestrian	Number of persons killed	1.218
	Number of persons injured	37.111
Total	Number of persons killed	5.229
	Number of persons injured	288.696

Table 3 shows that 7.99% of the traffic accidents in 2022 occurred at crosswalk and 0.39% at school crossings [7]. Although the accidents involving pedestrians are not only at crosswalks and the proportion of accidents occurring at pedestrian and school crossings in total accidents is quite low, the fact that pedestrians account for 23.2% of the deaths and 12.8% of the injuries in traffic accidents given in Table 2 is a situation that requires attention. It can be seen that accidents are concentrated in areas where the interaction between pedestrians and vehicles increases [8].

As can be seen from the table, fatal and injury accidents occur at a much higher rate in urban areas than in rural areas. However, the potential for vehicles to travel at higher speeds in rural areas may cause accidents to be more fatal.

Table 3. Traffic accident information with fatal and injury according to road type, 2022 [7]

	Residential area		Rural area		Total	
	Number	(%)	Number	(%)	Number	(%)
Crossovers						
Crosswalk	15.120	9,28	642	1,85	15.762	7,99
School crossings	742	0,46	30	0,09	772	0,39
Controlled rail crossing	302	0,19	16	0,05	318	0,016
Uncontrolled railway crossing	57	0,04	15	0,04	72	0,04
No crossings	146.446	90,03	33.891	97,97	180.337	91,42
Total	162.667	100	34.594	100	197.261	100

Accidents are unforeseen incidents that occur as a result of erroneous behavior. Accidents can occur for many reasons. When the causes of accidents (Table 4) are analyzed, it is seen that drivers have the largest share. Almost 9 out of every 10 accidents are caused by driver-related reasons. Unfortunately, driver errors can cause irreversible consequences. In addition to driver errors, although road and vehicle defects cause accidents, the other prominent factor is pedestrian errors. Almost 1 out of every 10 traffic accidents is caused by pedestrian errors [4]. Therefore, in order to effectively combat accidents, driver and pedestrian behaviors should be well examined and the factors that trigger errors should be identified. Thus, the risk of accidents can be reduced by eliminating the factors that cause accidents and making necessary improvements.

Table 4. Number of faults causing traffic accidents involving death or injury, 2013-2022 [4]

Year	Driver faults		Passenger Faults		Pedestrian faults		Road faults		Vehicle faults	
	Number	(%)	Number	(%)	Number	(%)	Number	(%)	Number	(%)
2013	162.327	88,7	774	0,4	16.458	9,0	1.913	1,0	1.558	0,9
2014	171.236	88,6	901	0,5	18.115	9,4	1.841	1,0	1.122	0,6
2015	187.980	89,3	915	0,4	18.522	8,8	1.916	0,9	1.165	0,6
2016	190.954	89,6	869	0,4	18.612	8,7	1.717	0,8	997	0,5
2017	191.717	89,9	782	0,4	18.095	8,5	1.619	0,7	1.112	0,5
2018	194.928	89,5	1.916	0,9	18.394	8,4	1.300	0,6	1.360	0,6
2019	180.042	88,0	2.572	1,3	16.726	8,2	1.045	0,5	4.153	2,0
2020	157.128	88,3	2.577	1,4	12.520	7,0	897	0,5	4.745	2,7
2021	195.382	87,1	3.941	1,8	18.398	8,2	936	0,4	5.761	2,6
2022	204.233	86,8	2.753	1,2	22.234	9,5	902	0,4	5.054	2,1

Although there are many factors in the occurrence of accidents, as seen in Table 4, pedestrian-related errors are an important cause. This situation reveals the necessity of pedestrian-oriented studies. Pedestrian behaviors effective in the occurrence of accidents were examined. Acting in a way that endangers vehicles on the roads has the highest rate of error in accidents caused by pedestrians with 29.6%.

Pedestrians trying to cross the road outside the designated areas where there are no crosswalk or intersections is also the leading cause of accidents with a rate of 27.3%. Pedestrians frequently cross the road where there are no crossings and without following the rules. In order to create a safer traffic infrastructure, it is important to manage crosswalk in a more planned manner and to raise awareness among pedestrians and drivers. Another important type of error is violating traffic lights and signals, such as crossing into the path of vehicles and violating traffic rules when crossing the road (Table 5) [4].

Table 5. Faults causing road traffic accidents involving death or injury, 2022 [4]

Pedestrian faults	Number	(%)
Violating crossing rules where crosswalk and junctions not exist	6.079	27,3
Violating traffic lights and signals	2.755	12,4
Acting behaviours on vehicle roads that endanger traffic vehicles	6.571	29,6
Violating traffic rules while crossing roads	209	0,9
Entering the vehicle road	474	2,1
Not walking on the left side of the vehicle road	245	1,1
Not taking accident preventing cautions where night and day vision is unclear	592	2,7
Other pedestrian faults	5.309	23,9
Total	22234	100

There are different types and methods of operation of crosswalks (Fig. 1). Crosswalks are divided into two as At-grade crossing and Grade-separated crossing, depending on the plane on which they are built. Grade-separated crossings are underpass and overpass. At-grade crossings are divided into controlled and uncontrolled [9].

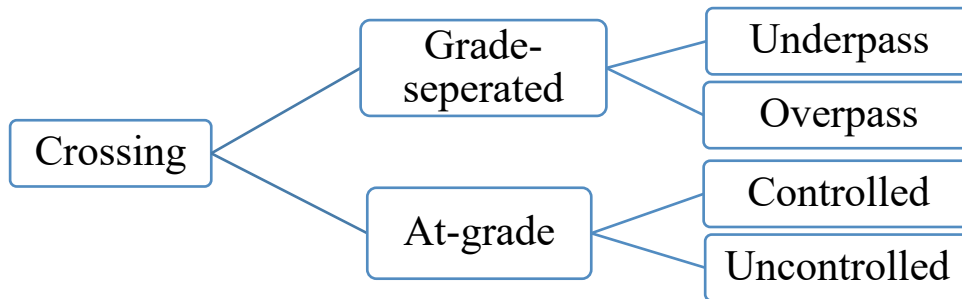


Fig. 1. Crossing operating modes [9]

Controlled crosswalk can be implemented with police supervision or by using signalization systems. It is not sustainable to manage all crosswalk with police supervision. Signalization is widely used in the operation of level and controlled crosswalks. Unlike crosswalks at intersections, supervised crosswalks along road axes are usually pedestrian-activated. When the pedestrian arrives at the crossing to cross the road, he/she activates the system by pressing the button on the signaling pole (Fig. 2). In line with the pedestrian's right of way request, the signaling system turns on a red light for vehicles and a green light for pedestrians within a certain period of time. Thus, pedestrians can safely cross the pedestrian crossing when the vehicles stop within the allotted time.



Fig. 2. Crosswalk button examples

However, there are some problems in the operation of pedestrian push-button signalization systems at crosswalks. First of all, pedestrians who do not know the working logic of the system try to cross the road when they find suitable intervals between vehicles without using the signalization system, which creates accident risks. Another issue is that pedestrians cross the street without waiting for the green light after pressing the button. In this case, while the pedestrian is completing the crossing or later, if the light turns green for pedestrians, the red light also turns red for vehicles, and vehicles continue to stop in vain after the pedestrian has finished crossing. In this scenario, vehicles will consume unnecessary fuel and emit unnecessary exhaust emissions, resulting in economic losses as well as environmental damage. In addition, the delay time of vehicles increases as a result of unnecessary stopping of vehicles.

Within the scope of the study, the failures occurring at pedestrian signalized crosswalks with pedestrian warning systems will be examined. As a result of the data obtained in line with pedestrian and driver behaviors, it is aimed to determine the operational problems in signalized crosswalks with pedestrian warning and to increase efficiency with the studies to be carried out. With a more efficient pedestrian crossing, it is aimed to increase pedestrian safety and reduce fuel consumption and exhaust emissions by eliminating unnecessary waiting for vehicles. In this direction, a pilot pedestrian crossing was determined and data on pedestrians and drivers were obtained through observations. The results show that there is potential for academic studies and field applications related to crosswalks.

1.1. Background

Crosswalks are areas arranged for the common use of vehicles and pedestrians with horizontal and vertical markings or traffic lights [13]. However, in developing cities, the vehicle-oriented service concept leaves pedestrians in the background [14]. The intersection of pedestrian and vehicle traffic brings potential risks. Based on this point, there are crosswalks and overpasses that aim to reduce accidents by separating pedestrian traffic from vehicle traffic [15].

Although pedestrian safety is a very important problem in developing countries such as Türkiye, it is generally not given importance [16]. Accidents may also occur due to inadequate or incorrect physical conditions of crosswalks [17-19]. Accidents can be prevented by establishing the right traffic management infrastructure [20].

In crosswalks, the absence or improper planning of signals for crosswalks also triggers accidents [21-23]. Similarly, the failure of pedestrians or drivers to comply with the existing signal planning or to use it correctly can also cause disruptions. Failure to fully know or recognize the rules also leads to violations [24].

In order to prevent traffic accidents at crosswalks and the negative consequences of these accidents, it is very important to correctly identify the factors that cause accidents. [25]. There are many studies examining pedestrian behavior at crosswalks, the factors determining crossing behavior and the effects of traffic conditions on behavior [26-29]. In these studies, pedestrian non-compliance with the rules is the leading cause of accidents. Pedestrian behavior may vary depending on many parameters. These differences may vary from country to country [30], or even in different cities within the same country [31,32]. For this reason, as in many traffic engineering problems, regional studies can be conducted on pedestrian-oriented issues and regional solutions can be developed. In this way, the traffic culture of that society can be better understood and the efficiency of the solutions developed will increase.

Failure of pedestrians to obey traffic lights eliminates the concept of controlled crosswalks. At this point, the reasons why pedestrians do not obey the rules should be examined well. Thus,

changes can be made and measures can be taken to ensure that pedestrians obey the rules in line with the reasons determined. When the reasons for pedestrians not obeying traffic lights in the literature are examined, the behavior of pedestrians being in a hurry comes first. The increase in the waiting time as a result of the long red light duration or the thought that pedestrians can cross safely without waiting due to low traffic volume increases light violations [33-35].

A smooth operational infrastructure at crosswalks can only be achieved if drivers, but especially pedestrians, fully comply with the rules. In order for pedestrians to fully comply with the rules, pedestrian behaviors, expectations and dissatisfaction should be well examined and necessary changes should be made accordingly. Pedestrian safety and crosswalks will continue to be an interesting area of research for researchers.

2. Data collection and evaluation

2.1. Determining the region and obtaining data

In order to investigate driver and pedestrian behaviors at pedestrian crosswalks with pedestrian push-button control, a pedestrian crosswalk with pedestrian push-button located on Atatürk Boulevard (D010 - Samsun Sinop road) in Körfez neighborhood of Atakum district of Samsun province was examined (Fig. 3). In determining this pedestrian crossing, observation of heavy pedestrian and vehicle traffic was effective due to the density of commercial enterprises around the region, the location on the crossing route to the beach, and the schools and Ondokuz Mayıs University campus around it.

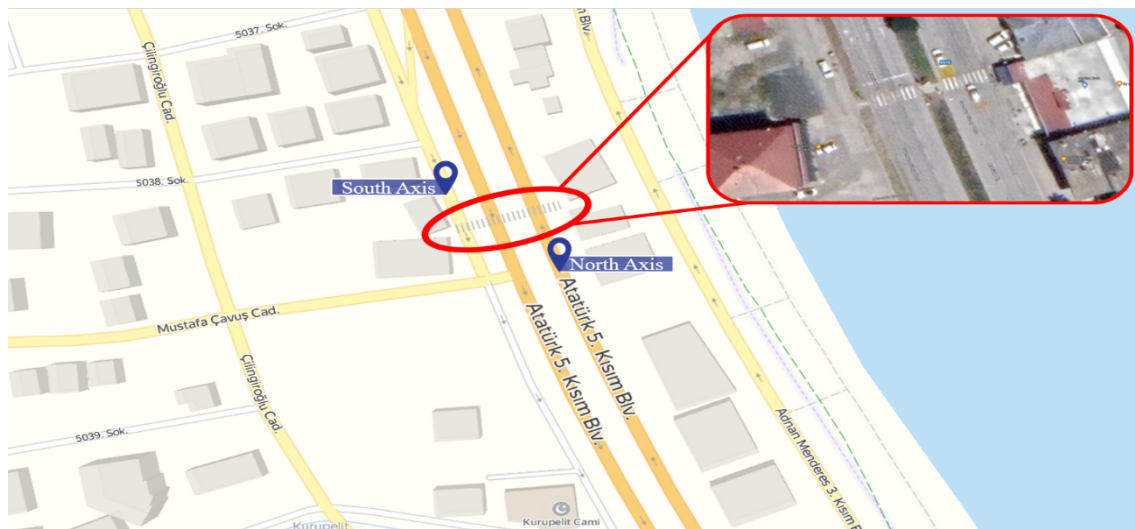


Fig. 3. Pilot area location [36-37]

In a study conducted to determine the traffic risk index of provinces in Türkiye, Samsun was found to be 65th risky in Türkiye [38]. Although this suggests that Samsun is one of the least risky cities in terms of traffic, the intense pedestrian and vehicle mobility, especially around Ondokuz Mayıs University and on the coastal line, brings various risks.

According to TÜİK statistics on the number of traffic accidents, deaths and injuries by provinces (2022), a total of 19,540 traffic accidents occurred in Samsun in 2022. 3,626 traffic accidents resulted in death or injury and 110 people died and 5,399 people were injured in these accidents [4]. In terms of the total number of traffic accidents, deaths and injuries, it is seen

that Samsun province ranks quite high in the list. The ratio of people killed and injured per accident is also higher in Samsun province compared to Türkiye average.

In the section where the pilot pedestrian crossing is located, both directions have 3 lanes each and the directions are named as north and south axes (Fig. 4). The distance required for pedestrians to cross the road is approximately 23 meters. The crossing speed of pedestrians at crosswalks varies according to age and gender [39]. Although there are many studies on pedestrian crossing speeds in the literature [40], it would be a better approach to take into account the current studies conducted in Türkiye, considering that pedestrian behavior varies from country to country. The average crossing speed of pedestrians at crosswalks is assumed to be 0.9 m/sec.



Fig. 4. Pilot area axes [37]

The pedestrian crossing in the pilot area is a pedestrian crossing with pedestrian push-button signalization control. At the starting point of the crosswalk in both directions and at the traffic island, there are pedestrian buttons (marked) as shown in Fig. 5. Pedestrian buttons are located at the starting point in both directions and at the traffic island. When pedestrians press the button to cross the street, the system is activated and vehicles are stopped with a red light while pedestrians are signaled with a green light to cross the street safely.



Fig. 5. Pilot area and crosswalk button

In order to examine pedestrian and vehicle behaviors at the pedestrian crossing with pedestrian warning control in the designated pilot area, video recordings were taken during peak hours (between 3.30 pm and 6.00 pm) when vehicle and pedestrian traffic is intense for 10 days. Pedestrian and vehicle behaviors from video recordings were manually examined by the researchers, the times were determined with a stopwatch and the images were converted into numerical data.

2.2. Examining pedestrian behavior

Within the scope of the study, the crossing movements of 227 pedestrians using the pilot pedestrian crossing were analyzed. Pedestrian crossing movements fluctuate during the day, such as fluctuations in traffic flow. The observations revealed that the number of pedestrian crossing usage increases during the rush hours of work and school (16.00-18.00). As a result of the observations made and the examination of the video recordings obtained, it was determined that 62 pedestrians out of 227 pedestrians using the crosswalk crossed the road without using the buttons placed to give pedestrians the right of way. While 48 of 62 pedestrians waited for the traffic flow to decrease without pressing the button, 14 pedestrians who did not press the button crossed the road directly without waiting. 165 pedestrians pressed the button and waited for the right of way to be granted to them (Fig. 6).

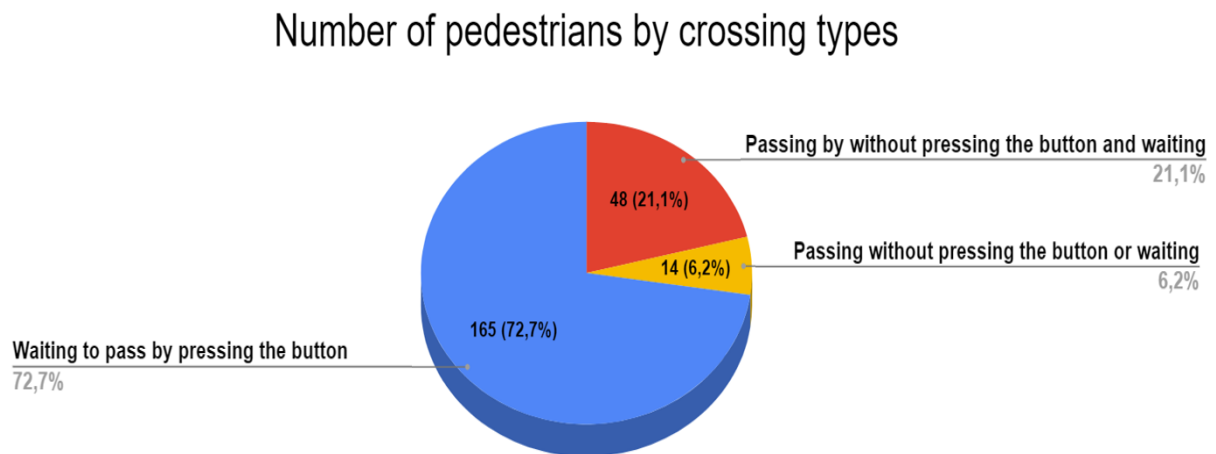


Fig. 6. Number of pedestrians by crossing types

In line with the data obtained, it can be said that the majority of pedestrians (72.7%) using the pedestrian crossing use the buttons. However, a significant portion (27.3%) do not use the buttons. In addition, there is a group of 21.1% who do not use the button even though they are waiting, which means that they do not have any knowledge about the working logic of the system. Although a large proportion of pedestrians cross safely by using the pushbutton, it is necessary to increase the rate of pushbutton use and to give pedestrians this habit. However, when the traffic density is not high, pedestrians may want to activate the system and cross the street at a convenient time without stopping the vehicles. In addition to lack of knowledge, this type of behavior can also be observed in pedestrians who do not use the button. Whether pedestrians do not want to use it or do not know the system cannot be fully determined by observations.

There were 165 pedestrians who crossed the street using the pushbutton at crosswalks, and the crossing movement was carried out in groups in a total of 67 times. Crossing movements were categorized and named according to the direction of crossing (Fig. 7).

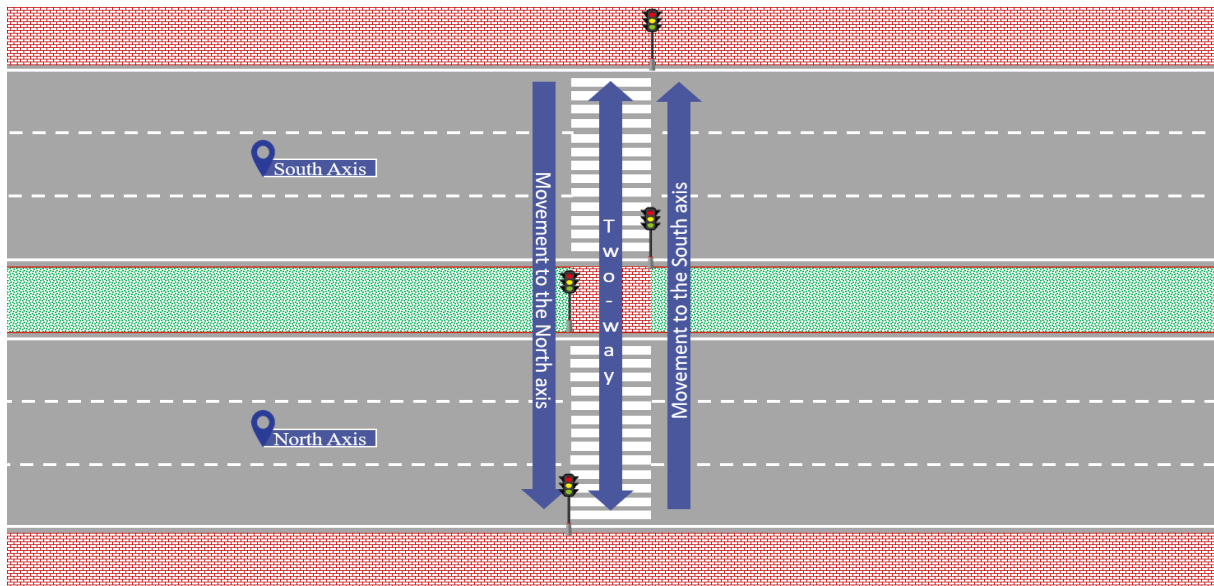


Fig. 7. Movement directions

Out of 67 different crossing movements, pedestrians crossed to the north axis 31 times and to the south axis 25 times. 11 crossings were observed in opposite directions (Fig. 8). It can be said that the lack of equal distribution according to directions is due to the surrounding places such as workplaces and beaches, as well as the traffic flow that changes directionally.

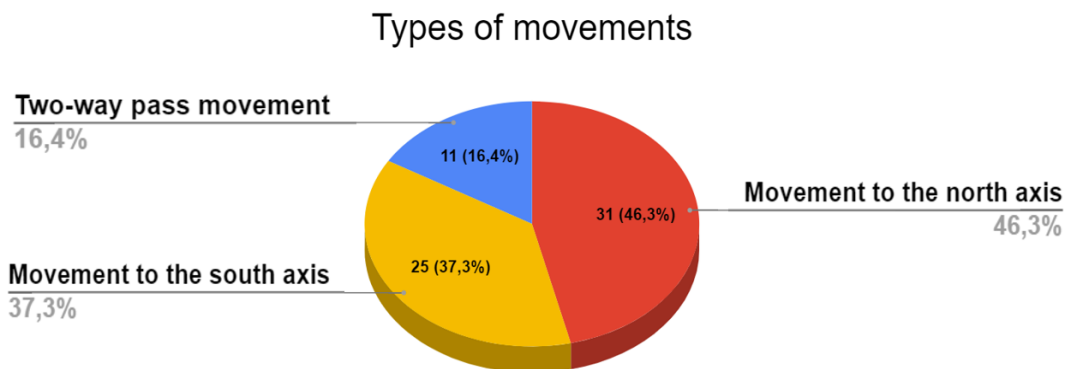


Fig. 8. Types of movements

It was also found that 83.6% of the crossings were one-way crossings. When pedestrians press the button in either direction, the red light for both axes is illuminated for vehicles. In other words, when pedestrians press the button on the south axis and cross to the north axis, and when pedestrians press the button on the north axis and cross to the south axis, vehicles turn red on both axes when pedestrians press the button. However, pedestrians are crossing gradually and it can be said that pedestrians are moving on only one axis at first. Vehicles on the other axis pause unnecessarily. For this reason, different or staggered circuit schemes can be applied on the axes if necessary.

Pedestrians' button pressing positions were also analyzed. Pedestrians pressed the button at the north or south starting point 51 times, while 16 times they crossed the first section without pressing the button and pressed the button at the traffic island. Similarly, when pushing the button at the traffic island, pedestrians benefit from the pause of vehicles to cross only one direction. However, the other direction unnecessarily waits at the red light. Unnecessary hesitation increases fuel consumption, exhaust emissions and delays. Unnecessary waiting can also create tension among drivers and trigger red light running.

In addition to drivers, the system also has drawbacks for pedestrians. At crosswalks with pedestrian warning signalization systems, after pedestrians press the button, a red light for vehicles and a green light for pedestrians turn on after a certain period of time and pedestrians have the opportunity to cross safely during this period. However, in 11 out of 67 observations, it was observed that pedestrians crossed the street before the green light turned on after pressing the button. Observations have shown that the green light for pedestrians turns on very shortly after the button is pressed. Pedestrians wanting to cross the street without waiting creates possible accident risks. In addition, there is a possibility that pedestrians may cross without using the button after waiting for a few seconds, while pressing the button unnecessarily stops the vehicles after they have crossed. These situations prevent the system from working effectively. In this direction, the system can be operated more efficiently with simple solutions such as pedestrians holding the button or waiting on an area on the ground where sensors are placed.

During the examination of the crossing movements at the pedestrian crossing, it was determined that the pedestrian push-buttons were used 67 times. When all rounds were analyzed, the average of 2 pedestrians crossed for each round, while the standard deviation value was found to be 1.5. For the 67 rounds of crossing movements, the parameters of the crossing movements such as the position of the button press, the position of the pedestrians when the light turns green for pedestrians, the number of pedestrians crossing in that round, the direction of the crossing movement, the waiting time for pedestrians and the segment in which the pedestrians crossed are analyzed and presented in Table 6.

Table 6. Obtained pedestrian movement data

Movement Number	Button Pressed Position	Position of the Pedestrian When It Turns Green	Number Of Pedestrians Waiting	Pedestrian Movement Direction	Waiting Time Of The Longest Waiting Pedestrian (sec.)	Average waiting time of pedestrians (sec.)	Did the pedestrian cross the green side? / *
1	Traffic Island	Traffic Island	2	North	11	11	Yes
2	Sidewalk	Road	3	North	4	4	No / 4
3	Sidewalk	Sidewalk	3	Two-way	10	8	Yes
4	Sidewalk	Sidewalk	3	South	8	8	Yes
5	Traffic Island	Traffic Island	2	North	21	21	Yes
6	Sidewalk	Sidewalk	2	South	10	10	Yes
7	Sidewalk	Sidewalk	2	South	9	9	Yes
8	Sidewalk	Sidewalk	1	South	9	9	Yes
9	Traffic Island	Traffic Island	1	North	12	12	Yes
10	Traffic Island	Traffic Island	1	North	8	8	Yes
11	Sidewalk	Road	1	South	3	3	No / 5
12	Sidewalk	Sidewalk	4	North	10	10	Yes
13	Sidewalk	Sidewalk	3	North	10	10	Yes
14	Sidewalk	Sidewalk	3	South	15	15	Yes
15	Sidewalk	Sidewalk	1	North	13	13	Yes
16	Sidewalk	Sidewalk	1	South	10	10	Yes
17	Traffic Island	Traffic Island	3	North	37	27,33	Yes
18	Sidewalk	Sidewalk	1	South	13	13	Yes
19	Sidewalk	Sidewalk	1	South	5	5	No / 5
20	Traffic Island	Traffic Island	1	North	9	9	Yes
21	Sidewalk	Sidewalk	5	Two-way	13	8,5	No / 2

22	Sidewalk	Sidewalk	2	South	8	8	Yes
23	Traffic Island	Road	3	North	5	5	No / 3
24	Traffic Island	Traffic Island	6	Two-way	20	15,33	Yes
25	Traffic Island	Traffic Island	3	North	16	16	Yes
26	Sidewalk	Road	2	Two-way	5	5	No / 4
27	Sidewalk	Sidewalk	1	South	19	19	Yes
28	Traffic Island	Traffic Island	5	North	20	20	Yes
29	Traffic Island	Road	4	North	11	11	No / 3
30	Sidewalk	Sidewalk	2	Two-way	10	10	Yes
31	Sidewalk	Sidewalk	2	North	8	8	Yes
32	Sidewalk	Sidewalk	1	North	9	9	Yes
33	Sidewalk	Sidewalk	6	North	26	16,6	Yes
34	Sidewalk	Sidewalk	7	North	25	16,67	Yes
35	Sidewalk	Sidewalk	2	North	8	8	Yes
36	Sidewalk	Sidewalk	1	North	9	9	Yes
37	Sidewalk	Sidewalk	3	Two-way	9	9	Yes
38	Traffic Island	Traffic Island	1	North	8	8	Yes
39	Traffic Island	Traffic Island	1	North	6	6	No / 3
40	Sidewalk	Sidewalk	1	South	8	8	Yes
41	Sidewalk	Sidewalk	1	North	7	7	Yes
42	Traffic Island	Road	2	North	3	3	No / 5
43	Sidewalk	Sidewalk	1	South	8	8	Yes
44	Traffic Island	Road	1	South	5	5	No / 3
45	Sidewalk	Sidewalk	3	North	8	8	Yes
46	Sidewalk	Sidewalk	4	Two-way	18	18	Yes
47	Sidewalk	Sidewalk	2	North	10	10	Yes
48	Sidewalk	Sidewalk	3	South	17	17	Yes
49	Sidewalk	Sidewalk	2	South	9	9	Yes
50	Sidewalk	Sidewalk	1	South	8	8	Yes
51	Sidewalk	Sidewalk	3	North	8	8	Yes
52	Sidewalk	Sidewalk	2	Two-way	8	8	Yes
53	Sidewalk	Sidewalk	5	North	11	11	Yes
54	Sidewalk	Sidewalk	2	South	16	16	Yes
55	Sidewalk	Sidewalk	2	South	12	12	Yes
56	Sidewalk	Sidewalk	5	North	8	8	Yes
57	Sidewalk	Sidewalk	1	South	8	8	Yes
58	Sidewalk	Sidewalk	2	South	8	8	Yes
59	Sidewalk	Sidewalk	5	Two-way	9	9	Yes
60	Sidewalk	Sidewalk	2	South	8	8	Yes
61	Sidewalk	Sidewalk	2	Two-way	8	8	Yes
62	Sidewalk	Road	5	Two-way	10	8,33	No / 3
63	Sidewalk	Sidewalk	4	South	8	8	Yes
64	Traffic Island	Traffic Island	1	North	9	9	Yes
65	Sidewalk	Sidewalk	3	North	51	24,33	Yes
66	Sidewalk	Sidewalk	1	South	8	8	Yes
67	Sidewalk	Sidewalk	3	South	8	8	Yes

* If the pedestrian crossed on red, how many seconds after it turned green?

During the 67 rounds in which the pedestrians activated the signalization system, the time they waited for the right of way to be granted to them was obtained. The average waiting time of pedestrians is 10.4 seconds for all rounds with a standard deviation of 4.78 seconds. Fig. 9 shows that the waiting times are much lower or higher than the average.

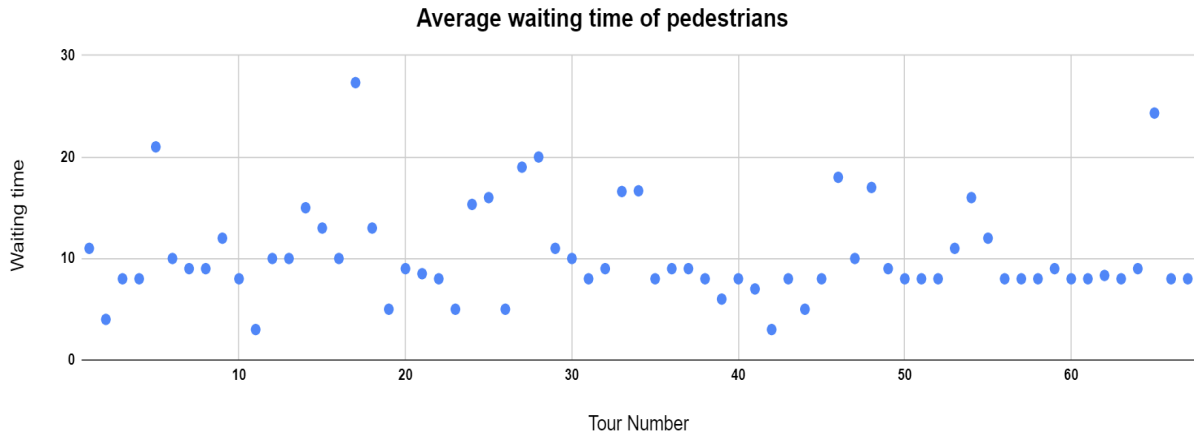


Fig. 9. Average waiting time of pedestrians

The longest waiting time for pedestrians waiting for a green light was also analyzed. The average waiting time for all rounds is 11.4 seconds with a standard deviation of 7.55 seconds. It can be seen from the data that although the waiting times are quite short, some rounds have high waiting times. More efficient and safer solutions for pedestrians should be developed with a more systematic pedestrian push-button signalization system.

According to the data obtained, 46.3% of the crossing movements in 67 different rounds were made on the north axis and 37.3% on the south axis. In 16.4% of the crossing movements, a two-way crossing was realized. In addition, pedestrians generally pressed buttons on the sidewalks at points that can be considered as starting points for crossing (76.1%). However, some pedestrians (23.9%) did not use the pushbutton on the first axis when the traffic flow was calm for crossing the street, but used the pushbutton when they reached the traffic island due to the heavy traffic flow on the other axis (Fig. 10).

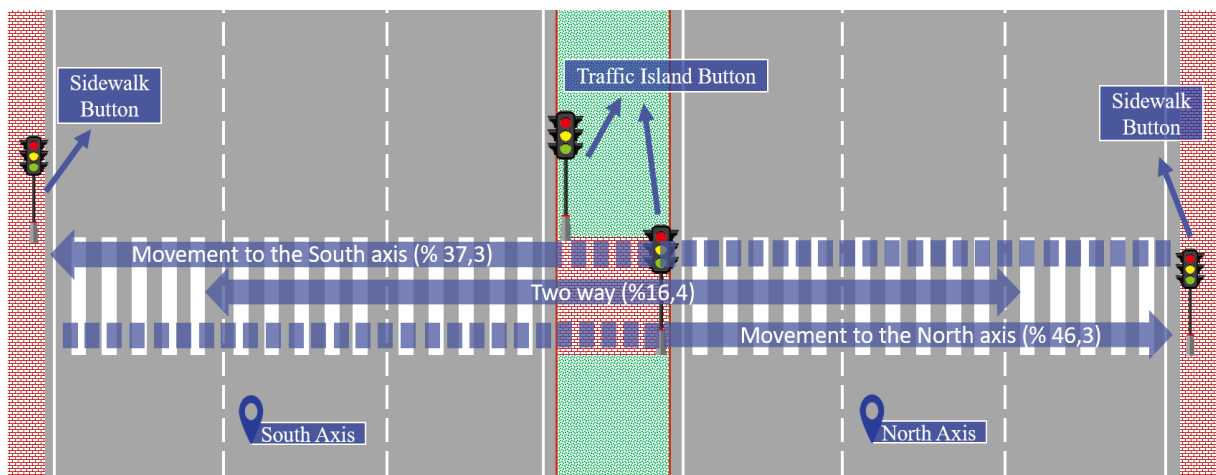


Fig. 10. Movement distribution according to movement directions

It has been observed that pedestrians tend to cross before the light turns green if there is a dilution in the traffic flow after pressing the button and there is an opportunity to cross. The locations of pedestrians who pressed the button when the light turned red for vehicles and green

for pedestrians were also analyzed within the scope of the study. 11.9% of the pedestrians did not wait for the green light to turn on and turned green when they were on the road platform. When the light turned green, 70.2% of pedestrians waited on the sidewalk and 12% waited on the traffic island.

2.3. Examining driver behavior

At crosswalks with pedestrian push-button signaling systems, a red light is turned on for vehicles at the same time as a green light is turned on for pedestrians to give pedestrians the right of way. Thus, vehicles are kept waiting for pedestrians to cross safely.

Within the scope of the research, a total of 791 vehicles were stopped due to red lights during the 67 rounds in which the system was activated. The information about the vehicles stopped at red lights (how many vehicles stopped, the waiting time of the first stopped vehicle, average waiting time) is given in Table 7.

Table 7. Obtained vehicle data stopping at the pedestrian crossing

Tour Number	Number of Vehicles Waiting at Red Light	Waiting Time for the First Vehicle to Stop (sec.)	Average Waiting Time of Vehicles for South Axis (sec.)	Average Waiting Time of Vehicles for North Axis (sec.)
1	10	25	14,5	15,00
2	4	24	11	20
3	7	25	23,67	16,25
4	10	23	7,5	15,50
5	8	23	10,5	14,75
6	9	25	20,75	20,00
7	9	24	13	18,67
8	6	25	12,25	19
9	11	13	11,88	10
10	3	18	18	13,5
11	8	25	13,6	18
12	9	23	14,57	18
13	7	24	15,8	21,5
14	8	25	23	15,29
15	22	25	15,87	16,33
16	12	25	9,57	13
17	16	26	16	15,75
18	15	25	19,69	9,5
19	18	25	17,5	16,5
20	11	24	9	15,33
21	7	25	10	18,6
22	4	18	6	15
23	4	21	13	14,67
24	12	25	19,33	19,67
25	16	26	16	15,75

26	4	22	12	16,67
27	20	24	13,58	21
28	7	24	3,67	15,75
29	23	25	14,17	0
30	18	25	17,00	22
31	24	26	16,45	18,75
32	4	24	14	24
33	16	25	7,57	17
34	13	24	18,33	7,25
35	18	26	18,56	14,5
36	21	26	17,39	11
37	5	25	9,67	22,5
38	23	25	16,37	19,5
39	18	21	13,31	8,5
40	10	26	18,29	10
41	10	25	9,40	19,6
42	21	25	19,07	0
43	18	25	15,93	23,3
44	5	21	0	15,4
45	4	18	0	11,5
46	7	27	21	14,33
47	14	27	7,5	18,33
48	8	22	12,17	14,5
49	4	22	22	17,67
50	3	19	11,5	19
51	0	0	0	0
52	14	23	15,69	11
53	12	26	7,67	20,17
54	8	15	12,5	13,5
55	9	23	12	18,8
56	17	26	14,62	11
57	21	25	17	15,17
58	17	24	16,08	18,8
59	16	22	14,33	12,5
60	19	7	14,67	3,75
61	21	8	15,33	13,6
62	19	25	18,53	10,5
63	5	17	16	11,67
64	20	25	18	19
65	15	23	13,64	22
66	5	24	0	15,8
67	9	23	5,67	16,83
Mean (\bar{x})	12	23	13,4	15,2
SD (σ)	6,29	4,8	5,4	5,1

SD (σ) : Standart deviation

As a result of the observations, average waiting time of vehicles for south axis was 13.4 seconds (SD=5.4) and average waiting time of vehicles for north axis was 15.2 seconds (SD=5.1). It was also found that an average of 12 vehicles stopped for each round and the first stopped vehicle waited at the red light for an average of 23 seconds. No vehicle waited at the red light for 3 rounds for South axis and 2 rounds for North axis. As a result of the observation, it can be said that the volume value for the south axis is higher than the north axis. It is thought that this is due to the fact that there is usually a movement of leaving work and returning to residential areas during the observation periods. The number of vehicles waiting at red lights during the rounds is given in Fig. 11.

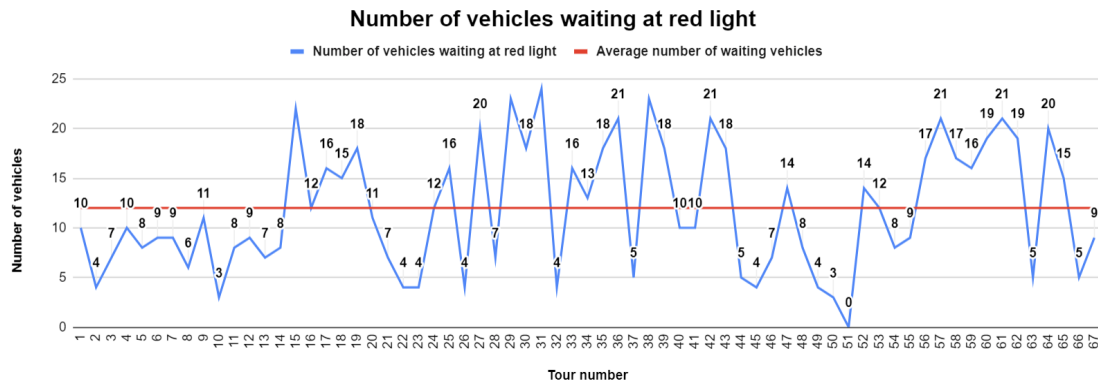


Fig. 11. Number of vehicles waiting at red light

In the observations made within the scope of the study, it was determined that an average of 12 vehicles paused at crosswalks as a result of the signalization system during all rounds. When the graph is analyzed, it is determined that 6 or less vehicles stopped at the lights in 15 rounds. This shows that on the road with 2 directions and 3 lanes, assuming that the vehicles are equally distributed directionally, an average queue of 1 vehicle is formed in each lane. In the 40 laps, 12 or less vehicles stopped at the lights. Similarly, on a 2-way and 3-lane highway, queue formation of 1 or 2 vehicles per lane can be mentioned. Queues of 1 or 2 vehicles are scenarios that do not constitute a major obstacle for vehicles to accelerate after a red light. However, as the number of stopped vehicles starts to increase as a result of the signaling system at crosswalk, a significant increase in delay values can be observed due to both the number of queues and acceleration.

In cases where a total of 19 or more vehicles were stopped for both directions, it shows that queue formation of 3 or more vehicles occurred on average in each lane on the road with 2 directions and 3 lanes, assuming that the vehicles are equally distributed directionally. When the delay data for these rounds are analyzed, it is found that the Average Waiting Time of Vehicles for South Axis value is higher than the average delay value obtained for all rounds in rounds with queues of 3 or more vehicles. However, the same is not the case for the north axis. In this case, it is thought that the inference that the volume value for the south axis is higher than the north axis, as emphasized earlier, is effective.

In order to determine the state of traffic flow, the distribution of the data obtained according to hours was realized (Fig 12). While examining the pedestrian crossing usage, it was determined that the number of crosswalks used by pedestrians increased during the rush hours of work and school (16.00-18.00). In parallel with the intensity of pedestrian crossing use, the number of vehicles waiting at crosswalks when the red light turns red for vehicles is considerably higher during these hours compared to other time periods.

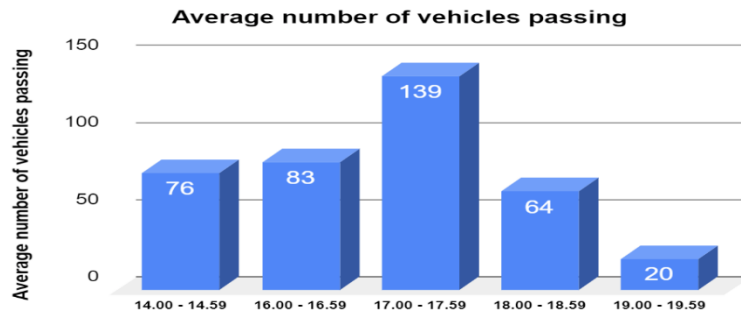


Fig. 12. Average number of vehicles passing

3. Conclusions and recommendations

In this study, pedestrian and driver behaviors at crosswalk with pedestrian push-button signalization control were investigated. In this context, data were obtained by making video recordings on different days and hours at the pilot pedestrian crossing determined in Samsun province. The crossing movements of 227 pedestrians using the crosswalk were analyzed. 165 pedestrians crossed the street using the pedestrian push-button in 67 different rounds. In this process, 791 vehicles in total paused due to the red light in 67 rounds when the pedestrians turned green and the vehicles turned red. In the studies conducted, pedestrians were not evaluated in terms of age and gender. For more comprehensive analysis, a study can be conducted that takes into account biological differences and psychological and behavioral differences in pedestrian behavior. In this way, the effective parameters in pedestrian behavior can be determined.

When the behaviors of pedestrians and drivers were analyzed, the following conclusions were reached.

- Although pedestrians generally use the pedestrian push-button, there are pedestrians waiting without using the button. It is thought that pedestrians may not know how the system works.
- Pedestrians using the button do not wait for the green light to turn green to cross the road, but cross when they find a suitable moment, and vehicles are stopped unnecessarily if the light turns green after crossing.
- If the button is pressed on the median, only one-way passage is provided and traffic is unnecessarily stopped on both axes.
- At one-way crossings, it may be unnecessary to stop traffic for both axes at the same time until the pedestrian reaches traffic island from the starting point.
- Unnecessary stops can create impatience for drivers and a tendency to run red lights.
- The green light duration defined for pedestrians was found to be appropriate based on the required duration calculated based on average pedestrian speeds and pedestrian crossing movements during observations.

In line with the results obtained, the suggestions developed for the system to work more effectively are presented below.

- Authorities should ensure that pedestrians understand the working logic of the system and encourage them to use it when necessary.
- Administrators should take measures to detect the presence of pedestrians in order to prevent unnecessary waiting of vehicles when pedestrians press the button but do not turn green. Simple solutions such as pressing the button or waiting in a defined area with sensors can be used. In addition, a mechanism should be added to make the button inactive in case of abandonment.
- A staggered or independent signal plan for the two axes can prevent unnecessary stops on both axes at the same time. If a button is pressed on the traffic island, pedestrians should be given a green light only for the axis in the direction of travel, not for both directions.
- If the system is used more efficiently, pedestrian safety will increase and unnecessary waiting for vehicles will be eliminated. Thus, decreases in fuel consumption and exhaust emissions can be seen. This is very important to provide a more environmentally friendly transportation infrastructure.

Acknowledgments

This study was conducted under a research project titled "i-gCar4ITS: Innovative and Green Carrier Development for Intelligent Transportation System Applications" which was supported by British Council. The authors would like to thank British Council for this support.

Author Contributions

Eren Dađlı: Conceived and designed the analysis, Contributed data or analysis tools, Performed the analysis, Wrote the paper.

Ahmet Gökтуğ Saraç: Collected the data, Contributed data or analysis tools, Wrote the paper.

Metin Mutlu Aydın: Conceived and designed the analysis, Contributed data or analysis tools, Performed the analysis, Wrote the paper.

References

- [1] Kıran, S., Şemin, S., and Ergör, A., Kazalar ve toplum sađlıđı yönünden önemi. *Sürekli Tıp Eđitimi Dergisi*, 10(2), 50-1, 2001.
- [2] Uyurca, Ö. and Atılgan, İ., Ankara ilinde meydana gelen trafik kazalarının incelenmesi. *Kent Akademisi*, 11(4), 618-626, 2018.
- [3] Akgüngör, A. and Dođan, E., Smeed ve Andreassen kaza modellerinin Türkiye uygulaması: Farklı senaryo analizleri. *Gazi Üniversitesi Mühendislik Mimarlık Fakültesi Dergisi*, 23(4), 2008.
- [4] Türkiye İstatistik Kurumu, Karayolu Trafik Kaza İstatistikleri 2022, 49513, 2023.
- [5] Dađlı, E., Aydın, M. M., Çoruh, E., Şehir İçi Ana Arterlerde COVID-19 Kısıtlamalarından Dolayı Trafik Akımlarında Meydana Gelen Deđişimlerin İncelenmesi: Antalya Örneđi. *İdealkent*, 12(34), 1199-1225, 2021.
- [6] Özen, M., Yaya kazalarının yaralanma şiddetinin incelenmesi: İkili lojistik regresyon modeli uygulaması. *Teknik Dergi*, 32(3), 10859-10883, 2021.
- [7] Karayolları Genel Müdürlüğü, Trafik Güvenliđi Dairesi Başkanlığı, Trafik Kazaları Özeti 2022, 2023.

- [8] Wong, S. C., Sze, N. N. and Li, Y. C., Contributory factors to traffic crashes at signalized intersections in Hong Kong. *Accident Analysis and Prevention*, 39(6), 1107-1113, 2007.
- [9] Mahmud, M.S., Pedestrian crossing behavior at intersections and existing walking facilities in Dhaka metropolitan city, Bachelor Thesis, *Bangladesh University Engineering and Technology Faculty*, 2015.
- [10] <https://www.slc.gov/transportation/walking/>, [Accessed: Jan. 10, 2024].
- [11] <https://sinyalizasyon.com.tr/sinyal-yaya-butonu-syb06>, [Accessed: Jan. 10, 2024].
- [12] <https://robertdyer.blogspot.com/2022/07/do-drivers-obey-pedestrian-crosswalk.html>, [Accessed: Jan. 10, 2024], 2022.
- [13] Sarısoy, G., Polat, A., Tezcan, H. O., Tramvay istasyonu erişimindeki işikli yaya geçidi ihlallerinin irdelenmesi, *TMMOB Elektrik Mühendisleri Odası, İnşaat Mühendisleri Odası, Makina Mühendisleri Odası Raylı Sistemler Kongre ve Sergisi*, Eskişehir, Türkiye, 2023.
- [14] Alkan, İ. N., Yeşil, M., yürünebilirlik kavramı ve çevresel faktörler odağında yaya kullanımı: Ordu - Akyazı mahallesi örneđi. *Akademik Ziraat Dergisi*, 11(2), 383-396, 2022.
- [15] Önelçin, P., Alver, Y., Üst geçit bölgelerinde kural dışı geçiş yapan yaya davranışlarının irdelenmesi ve yürüyen merdivenin üst geçit kullanım oranına etkisi. *Pamukkale Üniversitesi Mühendislik Bilimleri Dergisi*, 24(6), 1100-1106, 2018.
- [16] Uysal, M. and Alver, Y., Yükseltilmiş yaya geçidinin lise çağındaki yayaların kabul edilebilir aralık seçimine etkisi. *Pamukkale Üniversitesi Mühendislik Bilimleri Dergisi*, 27(3), 342-348, 2020.
- [17] Feliciani, C., Gorrini, A., Crociani, L., Vizzari, G., Nishinari, K., Bandini, S., Calibration and validation of a simulation model for predicting pedestrian fatalities at unsignalized crosswalks by means of statistical traffic data. *Journal of Traffic and Transportation Engineering*, 7(1), 1-18, 2020.
- [18] Pineda-Jaramillo, J., Barrera-Jiménez, H., Mesa-Arango, R., Unveiling the relevance of traffic enforcement cameras on the severity of vehicle-pedestrian collisions in an urban environment with machine learning models. *Journal of Safety Research*, 81, 225-238, 2022.
- [19] Sahu, P. K., Maji, A., Nath, B., Roh, H. J., Questionnaire based study of drivers' error and violation at four-legged signalized intersection. *Transportation Letters*, 2021, 1-12, 2021.
- [20] Ewing, R. and Dumbaugh, E., The built environment and traffic safety: A review of empirical evidence. *Journal of Planning Literature*, 23(4), 347-367, 2009.
- [21] Gitelman, V., Carmel, R., Pesahov, F., Evaluating impacts of a leading pedestrian signal on pedestrian crossing conditions at signalized urban intersections: a field study. *Frontiers in Sustainable Cities*, 2(45), 1-12, 2020.
- [22] Li, R. He, Y. L., T., Li, L., Schwebel, D. C., Huang, H. L., Yin, Q. Y., Hu, G. Q., Left-turning vehicle-pedestrian conflicts at signalized intersections with traffic lights: Benefit or harm? A two-stage study. *Chinese journal of traumatology*, 22(2), 63-68, 2019.
- [23] Simeunović, M., Jović, A., Pitka, P., Dobrić, M., The Impact of Uncertainty on Pedestrians' Decision to Start Roadway Crossing during the Clearance Phase. *Complexity*, 2021, 1-14, 2021.
- [24] Hatfield, J., Fernandes, R., Job, R. F. S., Smith, K., Misunderstanding of Right-Of-Way Rules at Various Pedestrian Crossing Types: Observational Study and Survey. *Accident Analysis & Prevention*, 39(4), 833-842, 2007.
- [25] Yaman, T., Dađlı, E., Aydın, M. M., Keleş, M. A., Fasılalı Geçiş Sistemlerinde Güvenli Geçiş Uygulamaları. *İdealkent*, 13(36), 797-823, 2022.
- [26] Hamed M., Analysis of pedestrians' behavior at pedestrian crossing. *Safety Science*, 38, 63-82, 2001.

- [27] Kadali R, Rathi N, Perumal V., Evaluation of pedestrian mid-block road crossing behaviour using artificial neural network. *Journal of Traffic and Transportation Engineering*, (2), 111-119, 2014.
- [28] Yannis G, Apadimitriou E., Theofilatos AA, pedestrian gap acceptance for mid-block street crossing, *WCTR 2010 World Conference on Transport Research Society*, Lisbon, Portugal, 2010.
- [29] Liu Y and Tung C., Risk analysis of pedestrians' road crossing decisions, effects of age, time gap, time of day, vehicle speed. *Safety Science*, 63, 77-82, 2014.
- [30] L. Hell, J. Sprenger, M. Klusch, Y. Kobayashi, C. Müller, Pedestrian behavior in Japan and Germany: A Review, *IEEE Intelligent Vehicles Symposium (IV)*, Nagoya, Japan, 2021.
- [31] İ. Küçükali, Understanding Pedestrian Road Crossing Behavior, Bachelor Thesis, *The Graduate School of Social Sciences Of Özyeđin University*, 2020.
- [32] Faisal, A. R., Kent Merkezi Ana Arter ve Kavşak Yaklaşımında Yaya Geçiş Davranışının İncelenmesi, Bachelor Thesis, *Süleyman Demirel Üniversitesi Fen Bilimleri Enstitüsü*, 2019.
- [33] Kruszyna, M., Jeremi Rychlewski, J., Influence of approaching tram on behaviour of pedestrians in signalised crosswalks in Poland. *Accident Analysis & Prevention*, 55 185-191, 2013.
- [34] Tiwari, G., Bangdiwala, T., Saraswat, A., Gaurav, S., Survival analysis: Pedestrian risk exposure at signalized intersections. *Transportation Research Part F*, 10(2), 77–89, 2007.
- [35] Lavalette, B.C., Tijus, C., Poitrenaud, S., Leproux, C., Bergeron, J., Thouez, J.P., Pedestrian crossing decision-making: a situational and behavioral approach. *Safety Science*, C47(9), 1248–125, 2009.
- [36] <https://yandex.com.tr/harita>, [Accessed: Jan. 11, 2024].
- [37] <https://www.google.com/maps>, [Accessed: Jan. 10, 2024].
- [38] Emniyet Genel Müdürlüğü, Trafik İstatistik Bülteni Kasım 2023, 2023.
- [39] Saplıođlu, M., Faisal, A. R., Sinyal kontrollü ve kontrolsüz kesimlerde yayaların karşıdan karşıya geçiş davranışlarının değerlendirilmesi. *Gümüşhane Üniversitesi Fen Bilimleri Dergisi*, 10(2), 309-320, 2020.
- [40] Highway Capacity Manual, Transportation Research Board National Research Council; 2010, 2010.